①

AD-A216 246

A COMPUTATIONAL MODEL FOR THICKENING
BOUNDARY LAYERS WITH MASS ADDITION
FOR HYPERSONIC ENGINE INLET TESTING

THESIS

Robert Douglas Clausen
Captain, USAF

AFIT/GAE/ENY/89D-04

DEPARTMENT OF THE AIR FORCE

AIR UNIVERSITY

AIR FORCE INSTITUTE OF TECHNOLOGY

Wright-Patterson Air Force Base, Ohio

89 12 29 027

AFIT/GAE/ENY/89D-04

A COMPUTATIONAL MODEL FOR THICKENING BOUNDARY LAYERS WITH

MASS ADDITION FOR HYPERSONIC ENGINE INLET TESTING

THESIS

Presented to the Faculty of the School of Engineering

of the Air Force Institute of Technology

Air University

In Partial Fulfillment of the

Requirements for the Degree of

Master of Science in Aeronautical Engineering

Robert Douglas Clausen, B.S.

Captain, USAF

December, 1989

Approved for public release; distribution unlimited

Preface

As the former leader of the National Aerospace Plane (NASP) Inlet Team, I saw that boundary layer simulation for inlet testing was a hurdle that needed to be overcome before the inlet flow field could be modeled accurately. Mass addition seems to be the most promising method to artificially generate a boundary layer. At the time of this writing, National Aerospace Plane inlet models are being tested with boundary layer injection systems which were designed empirically. The results of this thesis will add a theoretical aspect to that design process.

Software discussed in this report may be obtained from me at the Ballistic Systems Division, Norton AFB, CA. The best phone number that I can offer at this time is the Norton AFB operator's assistance, AV876-1110. Software may also be obtained from Mr Don Stava, current NASP Inlet Team leader, WRDC/FIMM, WPAFB OH, (513) 255-8508.

I would like to express my appreciation to my advisor, Lt. Col. Paul King. His expertise and thoroughness made this effort successful. I am also grateful to my sponsor, Don Stava, for his time and experience.

And most importantly, Thank You Carolyn. Thank you for everything that you've done for me and for enduring me while I endured AFIT.

Robert Clausen

ii

Distribution/		
Availability Codes		
Dist	Avail and/or Special	
A-1		

Table of Contents

List of Figures

List of Tables

List of Symbols

Cf_0	wall skin friction coefficient, p.6
C_p	specific heat at constant pressure, $ft \cdot lbf/(R \cdot slug)$
f	dimensionless y-transformation for the injection velocity profile
f_{up}	value of f at the upper edge of the injection velocity profile (lower edge of slipstream)
h	enthalpy, $ft \cdot lbf/slug$
l	height, ft
M	Mach
$\dot{m}$	mass flow per unit depth, $slug/(s \cdot ft)$
p	pressure, lbf/ft^2
R	gas constant, $ft \cdot lbf/(R \cdot slug)$
T	temperature, $^\circ R$
U	velocity, ft/s
u	x-component of velocity, ft/s
u_∞	free stream velocity, ft/s
$u+$	dimensionless velocity in the law-of-the-wall region
u_{up}	velocity at f_{up}, y_{up}, ft/s
V_w	effective injection velocity at station e, ft/s
v_0	y-component of velocity at the wall, injection velocity, ft/s
x	distance from leading edge, ft
xl	distance from leading edge to terminate boundary layer calculation and output data, ft
Y	height of the control volume in the integral momentum equation, ft
y	distance normal to plate, ft

y_{up} value of y at the upper edge of the injection velocity profile (lower edge of slipstream), ft

$y+$ demensionless distance from the wall in the law-of-the-wall region

Greek

δ contact surface ("wedge") deflection angle, degrees

δ_{99} boundary layer thickness at $u/u_\infty = .99$, ft

δ_1 dispacement thickness, ft

δ_2 momentum thickness, ft

δ_i injection angle, degrees

η blowing parameter, p.6

θ shock angle, degrees

λ_∞ injection mass flux parameter, p.6

ν kinematic viscosity, ft^2/s

ρ density, $slug/ft^3$

σ ratio of slipline (contact surface) width to length

τ_0 wall shear stress, lbr/ft^2

Subscripts

a   free stream

b   region behind shock above contact surface, Fig. 6

c   station at end of injection length, Fig. 6

d   region behind expansion above slipline, Fig. 6

e   station below slipline one l_e height downstream of c, Fig. 6

i   injection region

t   total

AFIT/GAE/ENY/89D-04

Abstract

A computational model for thickening boundary layers
with mass addition is developed. The phenomena of uniform
injection into a two-dimensional supersonic stream and
subsequent boundary layer growth downstream is discussed.
Analysis of the injection region provides the thickness of
the boundary layer just aft of injection. An injection
region velocity profile is then used to approximate the
boundary layer profile just aft of injection and is input
into a finite-difference boundary layer code. Downstream
profiles and thicknesses are calculated and compared to
experimental results.

The computational model developed here provides a tool
for the design of a boundary layer generation system for
hypersonic engine inlet testing. This mass addition system
is needed to simulate the boundary layer developed on the
forebody of hypersonic vehicles. An example is discussed
in which the natural boundary layer thickness is
increased 17 times.

ix

I. Introduction

The United States Air Force is currently pursuing a national program to develop the technology necessary to build a single staged aircraft capable of flying from conventional runways into orbit. This vehicle, the National Aerospace Plane (NASP), will use airbreathing propulsion to accelerate through hypersonic speeds to orbital velocities. In order to achieve the aerodynamic and propulsive efficiencies necessary to accomplish this goal, the vehicle forebody must be used as a precompression surface for the engine flowpath. This results in a thick boundary layer which must be bled-off or ingested by the engine. Current configurations under consideration for NASP will have boundary layer thicknesses at the inlet cowl station on the order of 20-30 percent of the cowl height (Stava, 1989).

In order to perform a wind tunnel test of an engine or inlet concept, large plates must be incorporated ahead of the inlet in order to simulate the boundary layer expected on the vehicle. Since the physical size of the model is limited by the test facility, the size of the inlet is forced to be very small in order to accommodate the length of the required extension plates. The small size of the inlet severely limits the amount of instrumentation and geometric features

1

that can be represented.

In order to demonstrate this difficulty and provide a useful example for later comparison, consider the boundary layer thickness on a hypersonic vehicle with a 100 ft forebody at a Mach 14, 120,000 ft flight condition (Figure 1). For a simple, single ramp forebody geometry the 99 percent boundary layer thickness may be estimated by (Schlicting, 1951:638)

$$\delta_{99} = 0.37 \ x \ \left(\frac{U_\infty \ x}{\nu}\right)^{-1/5} \tag{1}$$

to be 11.8 inches. For a typical inlet cowl height of about 3 ft, the boundary layer is 32 percent of this height. In order to test this configuration, a Mach 10 facility can be used with the boundary layer extension plates aligned parallel to the free stream in order to represent the conditions on the forebody surface (Figure 2). A suitable facility is the Naval Surface Warfare Center Mach 10, Nitrogen facility which has a large test rhombus allowing a model over 6 ft in length (Naval Surface Warfare Center, 1988). A 6 ft boundary layer extension plate in this facility would generate a boundary layer height of 0.50 inches. If this is to be 32 percent of the cowl height, the cowl height is only 1.5 inches! Imagine the difficulty trying to simulate internal inlet and engine geometry or incorporate instrumentation in this small size. The handicap of the boundary layer extension plates can be alleviated if a means exists to artificially thicken the boundary layer.

One such method is the use of mass addition (blowing) to create a thickened boundary layer. This concept would be comprised of a porous plate or a large number of small holes through which air is uniformly injected from a plenum below the plate (Figure 3). The porous section would be followed by a length of plate to allow the boundary layer profile to settle.

Both experimental and theoretical work has been done to study the effect of mass addition. Experimental efforts conducted in the 1960's concentrated on visualization of the streamline between the injected and free stream fluid and measurement of the injection surface pressure (Bott, 1967; Fernandez, 1968; and Hartunian, 1966). Theoretical analysis of the injection region has yielded streamlines, velocity profiles and pressures within the injection region (Lees, 1968 and Wallace, 1967 and 1968). None of this work was oriented towards thickening boundary layers and did not provide information on the flow field aft of injection. One test program (Rozycki, 1968) calibrate a mass injection system used for thickening boundary layers in a ramjet inlet test. This program provided velocity profiles downstream of injection, however, a generalized model for predicting downstream boundary layer thicknesses and profiles is still needed. Thus, the purpose of this thesis is to understand the injection phenomena and provide a generalized model which can be used to design boundary layer generator systems for hypersonic engine inlet testing.

II. Background and Phenomenological Effects

Three regimes exist as a function of injected mass flux for the two-dimensional problem of uniform injection into a supersonic stream. The first occurs when the injection term $(\rho_0 v_0 u_\infty)$ in the integral momentum equation (below) is comparable to or smaller than the skin friction term, τ_0 (Fernandez and Zukoski, 1968:1).

$$\tau_0 = \frac{d}{dx}\left(\int_0^Y \rho u^2 dy\right) - u_\infty \frac{d}{dx}\left(\int_0^Y \rho u dy\right) + \rho_0 v_0 u_\infty - \rho_\infty u_\infty Y \frac{du_\infty}{dx} \quad (2)$$

This type of flow results in a perturbation of the typical non-blowing velocity profiles with little boundary layer thickening.

Second, when the injection term is large compared with the skin friction term and the injectant mass flux is small compared to the free stream mass flux, the injection flow field consists of the following regions: a) an inviscid injectant layer, b) a shear layer interface with the free stream called the contact surface, and c) an inviscid external flow field (Wallace and Kemp I, 1967:2) (See Figure 4). The contact surface deflects the free stream flow as if it were a wedge.

Thirdly, when the injectant mass flux is significant compared to the free stream, the incoming boundary layer will completely separate resulting in an irregular flow field. The problem addressed in this report is solely the second regime since this is the only one that is capable of

4

generating a thickened boundary layer with a steady flow field geometry.

In order to quantify these three regimes, two parameters are useful. The first, $\eta = \dfrac{v_0}{u_\infty} Re^{1/2}$, appears in Kays and Crawford's similarity solution for the laminar incompressible boundary layer (Kays and Crawford, 1980:81). A value of η below 0.619 provides boundary layer solutions resulting from wall shear (flow regime 1). Values of η greater than 0.619 blow the boundary layer off the wall. Kays and Crawford's analysis pertains to incompressible flow. This study addresses the compressible problem however it is informative to compare the values of η for this study to $\eta = 0.619$. This study deals with η on the order of 1. - 250 which would indicate that the the flow field is well beyond regime 1.

The second parameter is the ratio of injectant mass flux to free stream mass flux, $\lambda_\infty = \dfrac{\rho_i u_i}{\rho_\infty u_\infty}$. If the integral momentum equation is nondimensionalized by free stream dynamic pressure, $\frac{1}{2} \rho_\infty u_\infty^2$, the injection term becomes $2 \cdot \lambda_\infty$ and the wall shear term becomes $\dfrac{\tau_0}{\frac{1}{2} \rho_\infty u_\infty^2} = Cf_0$, the skin friction coefficient. Although dependent on Reynolds Number, an average value of Cf_0 without mass injection is about $3\text{x}10^{-3} - 4\text{x}10^{-3}$ (Lees and Chapkis, 1968:3). This study deals with λ_∞ from 0.005-0.08. Since the nondimensionalized injection term, $2 \cdot \lambda_\infty$, is from 3 to 50 times Cf_0, the injection flow field type is regime 2 and wall shear can be

5

neglected in the analysis.

The upper limit on blowing rate for regime 2 occurs when the contact surface deflection angle, δ, becomes large enough to separate the incoming boundary layer (if present). Fernandez and Zukoski experimentally found this angle to be 14 degrees (Fernandez and Zukoski, 1968:3). In their test, blowing was conducted on the tunnel wall so an appreciable natural boundary layer was present ahead of the injection region. Without this incoming boundary layer, one would expect to achieve greater deflection angles before inducing separation because of the greater momentum near the wall. For the purpose of this study, it is advantageous to begin injection at the leading edge of the extension plate in order to minimize the overall length. Since no incoming boundary layer is present, angles greater than 14 degrees may be possible. However, since this is the only available data point for a separation limit, the upper limit on λ_∞ for regime 2 flow will be conservatively taken to be the value of λ_∞ which results in $\delta = 14°$.

Injection Region

In the injection region, Wallace and Kemp theoretically determined the geometry of the streamlines and found that they become closer near the contact surface (See Figure 4) (Wallace and Kemp I, 1967:34,35). This indicates that the fluid accelerates as it is forced into a smaller flow area by the fluid injected beneath it. These authors also found that

6

the pressure is constant in the y-direction and thus can be matched to the pressure at the contact surface produced by the external flow (Wallace and Kemp I, 1967:34). Fernandez and Zukoski's experimental results also confirmed the absence of any appreciable y-pressure gradient (Fernandez and Zukoski, 1968:3).

Injection may be accomplished with discrete holes or a porous material. Injectant velocities are a function of the pressure in the injection region unless the injection holes are choked. Very close to the injection surface, large spatial fluctuations in velocity were observed by Fernandez and Zukoski with both pitot and hot-wire probes. The fluctuations decayed rapidly with distance from the surface, and at a distance of 0.1 inches were within ±5 percent of the overall mean value. Most importantly, the overall mean injection velocity at the plate calculated directly from the hot-wire measurements agreed within ±5 percent with the values obtained by taking the measured total mass flow to the plate and dividing by the injection region density and the measured plate surface area. (Fernandez and Zukoski, 1968:2) Once the injection region pressure is determined, this allows the injection velocity to be readily calculated by

$$U_i = \frac{\dot{m}_i}{\rho_i l_i} = \frac{RT_i}{P_i} \frac{\dot{m}_i}{l_i} . \tag{3}$$

where $\dot{m}_i$ is determined by the choice of λ_∞.

Contact Surface

The injection fluid and the external fluid meet only in a thin, viscous, mixing layer at the dividing streamline called the contact surface. Static pressure and streamline inclination are continuous across the contact surface; velocity and temperature are discontinuous. In experiments, Hartunian and Spencer and J.F. Bott utilized a chemical reaction between the injected and free stream fluid to visualize the contact surface as shown in Figure 5. A major result was that the separation streamline was observed to be straight for all blowing rates. An exception to this is that, near the leading edge of the blowing, convex curvature could be observed (Hartunian and Spencer, 1966:1306). The curvature produces a normal shock in this small region which induces a high pressure on the plate that asymptotes quickly to a constant, greatly reduced value (Wallace and Kemp II, 1968:11). The small curvature at the leading edge of the straight contact surface encompasses, approximately, the first 0.6 inches of the injection length, l_i (Fernandez and Zuckoski, 1968:2). The injection lengths considered in this report range from 3 to 24 inches. The small leading edge curvature may influence the solution for the shorter injection length cases but the effect is most likely negligible for the longer lengths. Slight contact surface curvature is also present at the end of the injection region where the contact surface turns parallel to the wall. This

is shown in Figure 6. In order to simplify the analysis, the contact surface will be assumed to be straight.

The contact surface is actually a turbulent mixing layer of finite thickness which must match the velocities and temperatures of the outer and inner regions across its width. A gross measure of the contact surface thickness can be inferred from the photograph of Hartunian and Spencer's flow visualization experiments (Figure 5). The slip line grows approximately at a rate of 0.03 inches of width per inch of length or 3 percent. This thickness, however, is assumed to be zero for the injection region analysis but is included in the later boundary layer development analysis.

External Flow Field

The inviscid, external, flow field is deflected by the contact surface as if it were a wedge of equal deflection angle. Oblique shock relationships establish the flow conditions behind the shock and therefore set the pressure at the contact surface streamline and through the injection region down to the wall.

Aft of the injection region, the contact surface streamline turns and become a slip line parallel to the plate. The external flow passes through an expansion (Figure 6). Slip line angles not parallel to the plate are not steady state conditions for the flow aft of the injection region. Such a situation would cause the flow area below the contact surface streamline to change, resulting in pressure

differences above and below the slip line which would restore it to parallel. The pressure in regions d and e across the slip line must be equal since there is no flow across the slip line.

Mass Flow Balance

The key to solving the general problem of the injection region geometry lies in determining what phenomena governs the contact surface deflection angle, δ. Consider the mental experiment where injectant is instantaneously introduced into a supersonic stream at a constant λ_∞. All of the injected mass flow must pass through station e (See Figure 6) so the contact surface deflection angle will increase transiently until the injected mass flow can be accommodated at e. The conditions everywhere in the flow field are changing as a function of δ and, most importantly, the changing conditions at station e, along with the flow height, l_e, determine $\dot{m}_e$. Thus, the steady state contact surface deflection angle is established when $\dot{m}_e = \dot{m}_i$. This fact allows solutions for the contact surface deflection angle to be determined as a function of injectant mass flux parameter λ_∞.

The following analysis lends itself to two separate discussions, first, the modeling of the injection region and second, the calculation of boundary layer development downstream.

III. The Injection Region

Analysis

The goal of the injection region analysis is to calculate the contact surface deflection angle, δ, and the flow field conditions at each station as a function of injection mass flux parameter, λ_{∞}. Referring to Figure 6, flow field stations and regions are established as follows. Region a is the free stream condition. Region b is the inviscid region aft of the shock above the contact surface. Region d is the inviscid region aft of the expansion above the slip line. Station i represents the injection plane and is defined at the plane 0.1 in. above the injection plate where $U_i = \dfrac{\dot{m}_i}{\rho_i A_i}$ as previously discussed (Equation 3). Station c is at the end of the injection length. Station e is defined to be one $l_{\bullet}$ height downstream of station c and is assumed to be the point at which the irregular flow angles leaving station c have become parallel to the wall.

A control volume is established for the injection region from stations i to e (Figure 6). The control volume follows the contact surface, the slip line up to station e and along the wall of the injection region 0.1 in. above the surface. A few simplifying assumptions are necessary to render the problem tractable. 1) The shock and contact surface are assumed to be straight and attached at the leading edge of the injection region. 2) Shear forces are neglected on the contact surface. (Wall shear stress was previously shown to

11

be negligible for flow regime 2). 3) The flow height l_e is assumed to equal the geometric height $l_c = l_i \tan \delta$ (not depicted in Figure 6). The contact surface actually begins to turn just before the end of the injection region, as depicted in Figure 6, so l_e cannot be exactly known. Later results, however, show that the solution is not sensitive to l_e.

The following analysis of the two-dimensional flow field is one dimensional, i.e., flow field conditions represent averaged quantities. For the control volume, the continuity, axial momentum and the energy equations are given as Equations 4-6. Each mass flow term is per unit width.

continuity:

$$\dot{m}_i = \rho_e U_e l_e \tag{4}$$

axial momentum:

$$p_b (l_i \tan \delta) - p_e l_e = (\rho_e U_e l_e) u_e - \dot{m}_i U_i \cos \delta_i \tag{5}$$

energy:

$$\dot{m}_i (h_i + U_i^2/2) = (\rho_e U_e l_e)(h_e + U_e^2/2) \tag{6}$$

By making the following substitutions: perfect gas law for ρ, $l_e = l_c = l_i \cdot \tan \delta$, and $h = C_p T$, the three conservation equations become,

continuity:

$$\dot{m}_i = \frac{P_e}{R\,T_e}\, U_e l_e \tag{7}$$

axial momentum:

$$(p_b - p_e) l_i \tan \delta = \frac{P_e}{R\,T}\, U_e^2\, l_i \tan \delta - \dot{m}_i U_i \cos \delta_i \tag{8}$$

12

energy:

$$\dot{m}_i (C_p T_i + U_i^2/2) = \frac{p_e}{R T_e} U_e l_i \tan\delta \ (C_p T_e + U_e^2/2) \qquad (9)$$

Setting $p_e = p_d$ in Eq. 9 and solving for T_e,

$$T_e = \frac{p_d U_e^3 l_i \tan\delta}{2R\dot{m}_i (C_p T_i + U_i^2/2) - 2p_d U_e C_p l_i \tan\delta} \qquad (10)$$

Thus $T_e = T_e(U_e, \delta, \text{knowns})$. Substituting Eq. 10 into Eq. 8 and solving for U_e,

$$U_e = \frac{2\dot{m}_i (C_p T_i + U_i^2/2)}{(p_b - p_d + 2p_d C_p/R) l_i \tan\delta + \dot{m}_i U_i \cos\delta_i} \qquad (11)$$

Thus, $U_e = U_e(\delta, \text{knowns})$ only.

The test facility defines the free stream conditions, M_a, p_{ta} and T_{ta}. The designer specifies the injection system parameters: length of the injection region, l_i, injection angle, δ_i, and the value of λ_∞.

The following method is then used to find δ. This method is coded in the Fortran computer program *INJECT* (Appendix B) and is presented in flowchart form in Appendix A. The shock angle θ is first arbitrarily assigned a value of 10 degrees greater than the Mach wave angle. A unique δ can then be calculated (as opposed to the two solutions for θ as a function of δ) from oblique shock theory. The external flow field conditions (regions b and d) are then calculated using oblique shock and expansion theory.

13

Since $dp/dy \cong 0$ within the injection region, p_i is set equal to p_b. U_i is then calculated from Equation 3, repeated here,

$$U_i = \frac{\dot{m}_i}{\rho_i \, l_i} = \frac{RT_i}{p_i} \frac{\dot{m}_i}{l_i} \, . \tag{3}$$

The pressure at station e (p_e) is set equal to p_d and then U_e and T_e are calculated from Equations 11 and 10, respectively. The mass flow at station e is then calculated by

$$\dot{m}_e = \rho_e U_e l_e = \frac{p_e U_e l_i \tan\delta}{RT_e} \tag{12}$$

If $\dot{m}_e$ equals $\dot{m}_i$ (within a tolerance of $\dfrac{\dot{m}_i - \dot{m}_e}{\dot{m}_i} < 10^{-3}$), δ is found. If $\dot{m}_i$ is not within tolerance, θ is updated using a Newton-Raphson iterative method until δ is found. The value of $\dfrac{\dot{m}_i - \dot{m}_e}{\dot{m}_i}$ has only one root as a function of θ which facilitates iteration.

Results

Lambda was varied between values of 0.005 and 0.075 for Mach 2.6 free stream conditions and a 3.4 in. long injection region. These limits on λ_∞ ensure that the second regime of injection flow fields is obtained. The free stream and injection conditions used are the same as the tests conducted by Fernandez and Zukoski to allow for the comparison of results. Results of the analysis are summarized in Table 1 and graphically presented in Figures 7 and 8.

Figure 7 presents contact surface deflection angle δ and

injection pressure and velocity as a function of λ_∞. The contact surface deflection angle increases steadily with λ_∞ and reaches the 14 degree separation limit at a value of $\lambda_\infty =$ 0.07. Pressure in the injection region increases with injected mass flow and ranges from 1.2-2.5 times the free stream static pressure. The injection velocity increases with λ_∞ and ranges from only 1 to 7 percent of the free stream velocity. This indicates that the injectant momentum will be small relative to the free stream momentum.

Figure 8 presents the conditions at station e as a function of λ_∞. Since δ is relatively small, the loss in total pressure due to the shock is small. Thus, the equal angle compression and expansion results in p_d being nearly equal to the free stream value, as can be seen by the straight line in the figure. As λ_∞ increases, the velocity at station e increases to accommodate the additional mass flow as evidenced by the increase in M_e. The flow accelerates from the injection region to station e. The ratio U_e / U_i ranges from 24.3 to 7.75 for $\lambda_\infty =$ 0.005 to 0.075, respectively. T_e decreases with increasing λ_∞ because U_e is increasing and the thermal energy has been converted to kinetic energy.

The experimental results of Fernandez and Zukoski appear to be the only source of empirical data for δ as a function of λ_∞ with a similar geometry. Their Mach 2.6 tests used a 3.4 in. long porous plate with side walls projecting into the stream to preserve two-dimensionality. The contact surface

15

deflection angle was determined from schlieren shock angles and oblique shock theory. Contact surface deflection angle versus λ_∞ for the test data is shown by the solid line on Figure 9. Results of the analysis are shown by the dashed lines with the baseline case of $l_e = l_i \cdot \tan\delta$ as the center of the three dashed curves. The theoretical values provide good results at lower values of λ_∞. At higher values of λ_∞, the theoretical analysis predicts lower values than the experimental results. In order to find a possible explanation for this difference, the free stream and injection conditions were varied by ±10 percent to determine the sensitivity of the solution to these parameters. If the solution was sensitive to one or more parameters, an uncertainty in the given value may be significant enough to cause the difference. The results of the parametric variations are presented in Figures 9-14.

Figure 9 shows the effect of a ±10 percent change in l_e. One assumption in the analysis was that l_e equaled the geometric height $l_i \cdot \tan\delta$. This variation has little effect on the solution, especially at the upper values of λ_∞ and thus validates the assumption.

The ±10 percent variation of the free stream Mach number, Figure 10, has a moderate impact on the solution. The free stream Mach number affects the oblique shock pressure ratios and the value of $\dot{m}_i$ calculated from the given value of λ_∞. Ten percent variation in free stream temperature, Figure 11, has a limited effect. The effect of

16

varying T_a would be manifest by a change in the calculated value of $\dot{m}_i$. The variation of free stream pressure, Figure 12, has no effect on the solution which demonstrates that the solution is a function of pressure ratios and not absolute pressures. For a given λ_∞ and M_a, the pressure ratios throughout the flow field are constant and independent of variation in the magnitude of p_a.

Variations in injection conditions also had little effect. Variation of T_i directly affects the calculated value of $\dot{m}_i$ but did not significantly impact the values of δ as can be seen in Figure 13. A significant result is that the variation of the injection angle, δ_i, had almost no impact (Figure 14). The ratio of injectant momentum flux to free stream momentum flux ranges from 10^{-4} to 5×10^{-3}. Since the injected momentum is small compared to the free-stream, the direction of the injected momentum has little affect on the flow field. This indicates that injected momentum plays little part in establishing the contact surface deflection angle and supports the basic premise that conservation of mass drives this phenomena.

In summary, the solution of δ as a function of λ_∞ is not sensitive to the free stream or injection conditions. Thus, an uncertainty in the value of these conditions probably does not explain the difference in experimental and theoretical results at the higher values of λ_∞.

One possible explanation of this effect is the viscous interaction at the contact surface. Viscous forces would

17

create a thickened mixing layer at the contact surface with lower velocities than the inviscid region b velocity. This would create a displacement thickness that would effectively increase δ and the shock angle. J.F. Bott conducted similar blowing experiments and found that the effect of the interaction is to push the shock wave to a larger angle than would exist without the interaction (Bott, 1967:13). Figure 15 is a plot of shock angle as a function of effective wedge angle for Bott's experimental results and for oblique shock theory. In all cases, the experimental shock angles were above the theoretical.

A second possible explanation of the difference between the experimental and theoretical results is the curved contact surface at the leading edge of the injection region. The curvature displaces the entire contact surface in the y-direction before the linear contact surface begins. By neglecting the curvature, this displacement is not accounted for in the analysis.

A third explanation is perhaps that some anomaly exists in the test. The side walls, for example, will develop small boundary layers that will displace flow within the injection region. The contact surface would be pushed to a slightly higher angle to accommodate the fluid displaced by the side wall boundary layers. The actual effect is most likely a combination of the three possible explanations. The theoretical model however, does provide a reasonable model of the injection phenomena.

IV. Boundary Layer Development

Analysis

For the region aft of the injection, the goal is to incorporate the results of the injection region analysis into a boundary layer code and determine boundary layer heights and profiles at a desired location downstream. Station e serves as the starting location for the development of the boundary layer. The one-dimensional analysis of the injection region yielded a single averaged value for the velocity and temperature at station e. This uniform value was input into a finite-difference, boundary layer code as a uniform profile. The velocity and temperature profiles at station e are highly non-uniform however and a more accurate downstream profile may be obtained by using a more realistic representation of the starting profile. The actual flow field in region e is extremely complex and cannot be discerned without a computational analysis using the full Navier-Stokes equations. However, we can obtain a form of the velocity profile from previous work describing the flow field within the injection region.

Wallace and Kemp mathematically analyzed the flow field within the injection region for incompressible flow using a stream function approach. Their result for the velocity profile is (Wallace and Kemp, 1967:33)

$$u = V_w \cdot (1 - f - 2c \ln f)^{1/2} \qquad (13)$$

19

where u is the x-component of velocity, V_w is the injection velocity at the wall, $c = \dfrac{\pi}{2\delta^2}$ and f is a transformation of y given by $y = l_e(1-f)$. The value of f is defined as unity at the wall and zero at the contact surface and is taken to vary linearly between the two. A plot of Equation 13 (with f transformed to y) is shown in Figure 16. At the wall u = 0 and at the contact surface u approaches infinity. Although Equation 13 was derived for incompressible flow, the authors compared the incompressible streamlines to those for the compressible case and found them to be almost indistinguishable (Wallace and Kemp, 1967:33).

Since the contact surface slip line is a viscous mixing region of finite thickness, the actual velocity never approaches infinity. As previously discussed, the contact surface thickness at any given x-location is approximately 3 percent of the length. The lower half of this thickness would occupy the upper portion of the injection flow field region governed by the 'f' velocity function (Equation 13). The lower edge of the contact surface thickness defines the upper most value of f (f_{up}) (See Figure 16). For a given value of V_w and f_{up}, the velocity at f_{up} (u_{up}) is known from Equation 13. The velocity profile across the contact surface thickness must match the velocity (u_{up}) and the slope (du/df) at the lower edge and the region b velocity (U_b) with slope du/dy=0 at the upper edge. A third order polynomial is used to model the velocity profile through the contact surface

thickness and these four conditions are used to determine the coefficients of each term.

The total enthalpy in the injection region is given by $h_{t_i} = C_p T_i + U_i^2/2$ and is constant along a streamline. The temperature within the injection region is determined by $T(f) = (h_{t_i} - u^2(f)/2)/C_p$. The temperature through the contact surface thickness is also modeled by a third-order polynomial with the temperature and temperature gradients matched at the edges. This is presented graphically in Figure 17.

The 'f' function and third-order polynomial model applies to the profiles within the injection region; however, velocity and temperature profiles are required at station e in order to begin the boundary layer analysis. The injected fluid accelerates from station c to e but it would seem reasonable to assume that the form of the velocity profile at station e is similar to that in the injection region. Thus, this model is applied at station e. Since station e is aft of the injection region, V_w no longer has physical significance but is only a parameter which allows the model to be applied. In order to solve for the profile at station e, V_w is assumed and $u(f)$ and $T(f)$ in the lower region and $u(y)$ and $T(y)$ through the slip line are determined. The mass flow is then calculated by numerically integrating the profiles as follows:

$$\dot{m} = \dot{m}_{f\ profile} + \dot{m}_{slipline}$$

$$= \int_{1}^{f_{up}} \frac{p_e l_e u(f)}{RT(f)}\ df + \int_{y_{up}}^{le} \frac{p_e u(y)}{RT(y)}\ dy \qquad (14)$$

The mass flow is then compared to $\dot{m}_e$ and V_w is iterated upon until the mass flow equals $\dot{m}_e$ ($=\dot{m}_i$). The resulting profile is then input as the starting profile in the boundary layer code.

This profile, by definition, conserves mass at station e. However in order to be valid, momentum and energy must also be representative of the values calculated from the averaged, 1-D quantities. Momentum and energy are numerically integrated at station e in the program *INJECT*. For the Mach 2.6 case previously discussed and for a Mach 4.38 and Mach 10 case to be discussed, the difference between the 1-D and 'f' profile momentum were 10.9%, 11.3% and 15.4% respectively. The difference between the 1-D and 'f' profile energy was 0.0%, 0.3%, and 12.6% respectively. Although it is not possible to accurately conserve all three quantities, these differences are low. Thus, the 'f' profile satisfactorily represents the 1-D momentum and energy at station e.

The station e velocity and temperature profiles are now input into a boundary layer computer code. The code used is *TEXSTAN*, an updated version of STAN5 by Kays and Crawford. The code provides a finite-difference solution of the boundary layer equations and is used here to solve the

22

problem of turbulent boundary layer growth on a flat plate
with zero pressure gradient. The Reynolds number at station e
was calculated for the Mach 2.6, 4.38 and 10.0 cases and was
found to be 9.3×10^5, 4.2×10^6 and 8.4×10^7 respectively. Since
these values are greater than the external transition
criteria of 5×10^5, TEXSTAN is begun in the turbulent mode.
The *TEXSTAN* "law-of-the-wall" option (Crawford and Kays,
1976:25) is used to speed calculation. The edge of this
region ($y+ = u+ = 10$.) is calculated in the *INJECT* subroutine
YLAWDF.

Results

The injection region analysis was conducted at Mach 2.6
because of the availability of the Fernandez and Zukoski data
for δ versus λ_∞. However, they did not measure velocity
profiles downstream. The following analysis is conducted at
Mach 4.38 because of the availability of downstream profiles
from Rozycki's test program.

Boundary layer development for the uniform and 'f'
function starting profiles are compared in Figure 18. For
the Mach 4.38 conditions, the initial profile and the
profiles at 3 downstream locations, 6, 12 and 18 l_e heights
downstream, are presented. The solid curves represent
profiles originating from the uniform profile, the dashed
curves represent profiles originating from the 'f' function.
For the uniform starting profile, the "law-of-the wall"
region may be seen at the bottom of the profile and the

23

third-order polynomial may be seen at the top joining the uniform station e velocity to the higher region d velocity through the slip stream. In just six boundary layer heights downstream, the uniform profile has already resolved itself to the form of the 'f' function profile due to the high velocity gradients at the top and bottom of the starting profile.Thus, the use of the 'f' function does not significantly reduce the length of the plate aft of the injection region needed to stabilize the boundary layer. However, the uniform starting profile predicts greater boundary layer thicknesses due to the large velocity gradients at the top of the profile.

The boundary layer thicknesses are more accurately compared using the displacement thicknesses which are indicated on Figure 18 by squares. The displacement thickness clearly grows downstream and the uniform profile displacement thicknesses are greater than the 'f' profile thicknesses in each case.

In order to validate the estimated 3 percent value of slip line thickness, the effect of slip line thickness on boundary layer development was investigated. Results are presented in Figure 19 for Mach 4.38 conditions. The thickness growth parameter, σ, is varied from the baseline 3 percent up to 7 percent. The boundary layer height increases with σ since this parameter directly increases the thickness of the starting profile; however, for a 130 percent increase in σ, the boundary layer height increases only 6

percent. The profile shapes are almost identical. Thus, boundary layer development is not sensitive to the assumed value of slip line thickness. The original value of 3 percent is therefore used throughout this study.

Apparently only one set of experimental data is available for the profiles aft of the injection region. In a research program (Rozycki), a ramjet inlet was forced to ingest the missile forebody boundary layer. Inlet testing was done at the Air Force Academy's 12x12 inch cross section facility which did not have adequate length to reproduce the missile forebody boundary layer. Boundary layers were simulated using mass injection and profiles were measured with pitot rakes 11 in. downstream of injection (Figure 20). Profiles for a Mach 4.38 test are shown in Figure 21 and Rozycki has arbitrarily laid power law profiles through the data. The circles represent the no blowing case. Two blowing cases are plotted, the first, with δ_{99}= 0.627 inches is 2.53 times the non-blowing height and the second, with δ_{99}= 0.508 inches, is 2.02 times the non-blowing height. The data reasonably fits the power laws except near the wall where, contrary to intuition, the flow has higher velocities than a non-blowing boundary layer with the same thickness. Apparently, between station c and e (this report's notation) the flow rapidly accelerates near the wall.

The velocity profiles from this study can be compared to Rozycki's data based on the same 99 percent boundary layer height but not based on the same injected mass flux because

25

the author made an error determining it. The author had available vendor information for the porous plate mass flux as a function of Δp across the plate. For Δp, the author used the difference between plenum pressure and free stream static. The actual pressure within the injection region can be typically double the free stream value and thus would have yielded about half the mass flux.

Figure 22 compares the experimental data with the profiles resulting from the 'f' and uniform starting profiles. The mass flow parameter λ_{∞} was varied using *INJECT* until the 99 percent boundary layer profile matched the data. For δ_{99}= 0.627", the 'f' profile compares well with the data except near the wall. For δ_{99} = 0.508", profile agreement is good in the upper profile but again falls off near the wall. The uniform profile does not represent the experimental profiles well.

The goal of this thesis is to develop a general model for predicting thicknesses and profiles resulting from mass addition. In the Introduction, a Mach 10, Nitrogen, inlet test was considered which required 6 feet of extension plates to generate a 0.5 in. boundary layer for use with a 1.5 in. cowl height. The computational model developed in this report can now be used to model the artificial thickening of the boundary layer to illustrate the use of mass addition. The design variables are the length of the injection region, l_i, the injected mass flux parameter, λ_{∞}, and the length of the plate aft of injection to stabilize the profile.

Nitrogen is injected into the Nitrogen free stream. Retaining the overall plate length of 6 ft, λ_∞ is varied until δ reaches the 14 degrees separation limit. Lambda is held at this value. The injection length can then be varied to achieve various thicknesses since the starting boundary layer height (l_e) is geometrically $l_i \cdot \tan\delta$. Figure 23 presents boundary layer profiles at 6 ft for injection lengths of 0.5, 1.0 and 2.0 ft. The 0.50 in. boundary layer height result from the Introduction is plotted for comparison. Boundary layer thicknesses of 7, 11, and 17 times the non-blowing thickness are obtained, respectively. One might expect a 1/7 power law profile for a non-blowing turbulent boundary layer so these are shown for the same 99 percent thickness. The velocities in the injection boundary layer are lower than the 1/7 power law velocities. The shape of the injection profiles does not appear to change downstream. These profiles, having a change in concavity, resemble boundary layer profiles for flows in a adverse pressure gradient (White, 1974:470); however, no pressure gradient exists. The corresponding temperature profiles are presented in Figure 24.

27

V. Conclusions

This work has shown that the phenomena of uniform injection into a supersonic stream can be modeled and predicted. The phenomena is driven by a conservation of mass in the injection region and is not sensitive to changes in the free stream or injection conditions. The finite thickness of the viscous contact surface and leading edge curvature have the effect of increasing the contact surface deflection angle. The injection region ('f') velocity profile predicts the boundary layer thickness more accurately than a simple uniform profile. The boundary layer thicknesses are not sensitive to the initial assumptions for the slip line thickness. The predicted boundary layer profiles resemble the injection profiles of Rozycki, however, injection profiles do not resemble the 1/7 power law turbulent profile (A means of rectifying this problem is proposed as the second recommendation).

The modeling of this complex flow phenomena has been made tractable by some assumptions and simplifications. Sufficient accuracy has been obtained however to provide a useful tool for the design of boundary layer generators. This model allows the designer to size the system. Any inaccuracies can be compensated for during actual testing by monitoring a boundary layer rake and adjusting the injection mass flow accordingly.

VI. Recommendations

Two areas are suggested for further study. The first is the effect of the turbulent mixing thickness at the contact surface in the upstream, injection solution. This could be analyzed by modifying the boundary layer code for two free streams and applying it to the contact surface conditions. One problem would be the starting conditions. The 3 percent thickness and third order polynomial profile could be used as inputs to begin the solution.

A method of solving this problem might be as follows. First, *INJECT* would be run in its current form to provide the conditions in the injection region and region b. Region b provides a uniform upper boundary condition for the viscous code. The lower boundary condition would be a function of the viscous layer width since y_{up} would change as a function of x. Thus, the boundary condition at the lower edge of the contact surface thickness would have to be evaluated at each space step. Once the profile and thickness of the viscous layer is determined, a displacement thickness would be calculated and added to the contact surface deflection angle in a second run of *INJECT*. The process would then be repeated until little change in the solution is noted.

The second recommendation for future effort is to devise a method and computational model to manipulate the injection boundary layer profiles to more accurately model the

29

non-blowing 1/7 power law profiles. This might be accomplished by inserting rows of holes aft of the existing injection region which injected high momentum flow angled downstream to "fatten up" the injection profile. Aft of this row, an upstream facing row is needed to slow the profile near the wall.

Bibliography

Billig, F.S., Orth, R.C. and Lasky, M. "A Unified Analysis of Gaseous Jet Penetration," *AIAA Journal*, Vol. 9, No. 6, June 1971, pp. 1048-1058.

Bott, J.F. *Massive Blowing Experiments*, Contract AF 04(695)-1001. Aerospace Corporation, June 1967 (AD656705).

Crawford, M.E. and Kays, W.M. *STAN5 - A Program For Numerical Computation of Two-Dimensional Internal Boundary Layer Flows*. Contract NGR-05-020-134. Stanford University, December 1976 (NASA CR-2742).

Fernandez, F.L. and Zukoski, E.E. "Experiment In Supersonic Turbulent Flow With Large Distributed Surface Injection," *AIAA 6th Aerospace Sciences Meeting*. January 1968, No. 68-129.

Hartunian, R.A. and Spencer, D.J. "Visualization Technique for Massive Blowing Studies," *AIAA Journal*. Vol. 4, No. 7, July 1966, pp. 1305-1307.

Kays, W.M., and Crawford, M.E. *Convective Heat and Mass Transfer*. New York: McGraw-Hill Book Company, 1980.

Lees, L. and Chapkis, R. "Surface Mass Injection at Supersonic and Hypersonic Speeds as a Problem In Turbulent Mixing: Part I. Two-Dimensional Flow," *AIAA 6th Aerospace Sciences Meeting*. January 1968, No. 68-130.

Naval Surface Warfare Center. *Hypervelocity Wind Tunnel # 9: Test Planning Guide*. NSWC-MP-88-200 (Unofficial), Silver Spring, MD. 1988.

Rozycki, R.C. and others. *Experimental Development of Inward-Turning Air Inlets Designed For Mach 4.5*. Martin Marietta Corporation, June 1968.

Schlichting, H. *Boundary-Layer Theory*. New York: McGraw-Hill Book Company, 1951.

Stava, Donald, National Aerospace Plane Inlet Team Leader. Personal Inteviews. Flight Dynamics Laboratory, WRDC/FIMM, Wright-Patterson AFB OH, 1 June through 14 Dec 1989.

Wallace, J. and Kemp, N.H. Analytic Solutions To The Massive Blowing Problem: Part I: Similarity Solutions. Contract DA-10-021-AMC-12005. Avco Corporation, Everett,MA, October 1967 (AD823632).

Wallace, J. and Kemp, N.H. "Analytic Solutions To The Massive Blowing Problem: Part II: Thin Layer Analysis With Constant Blowing," AIAA 6th Aerospace Sciences Meeting. January 1968, No. 68-128.

White, F.M. Viscous Fluid Flow. New York: McGraw-Hill,1974.

Zucrow, M.J. and Hoffman, J.D. Gas Dynamics. New York: John Wiley & Sons: 1976.
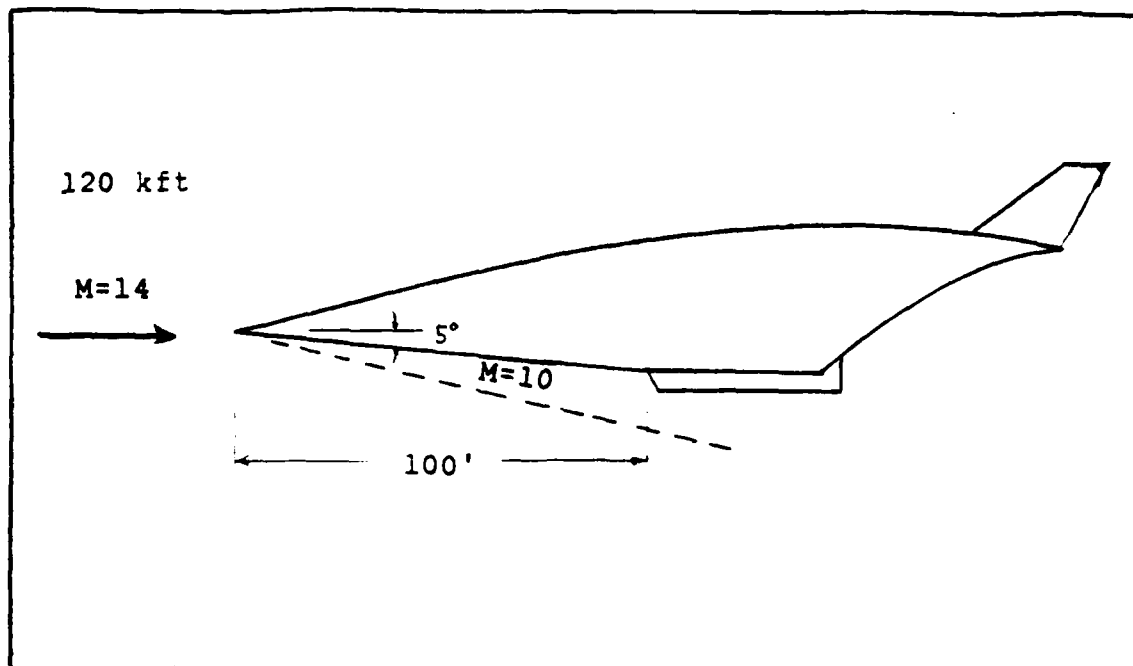
Fig. 1 Hypersonic vehicle with a single ramp forebody.
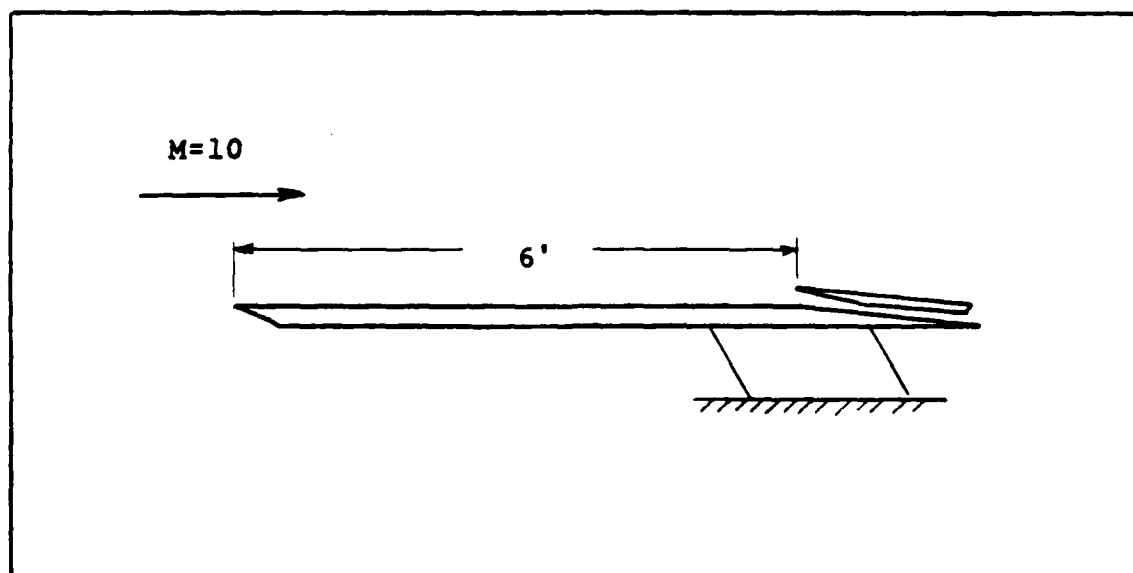
Fig. 2 Inlet Test model with 6 ft extension plate
used to create a representative vehicle
forebody boundary layer.

33
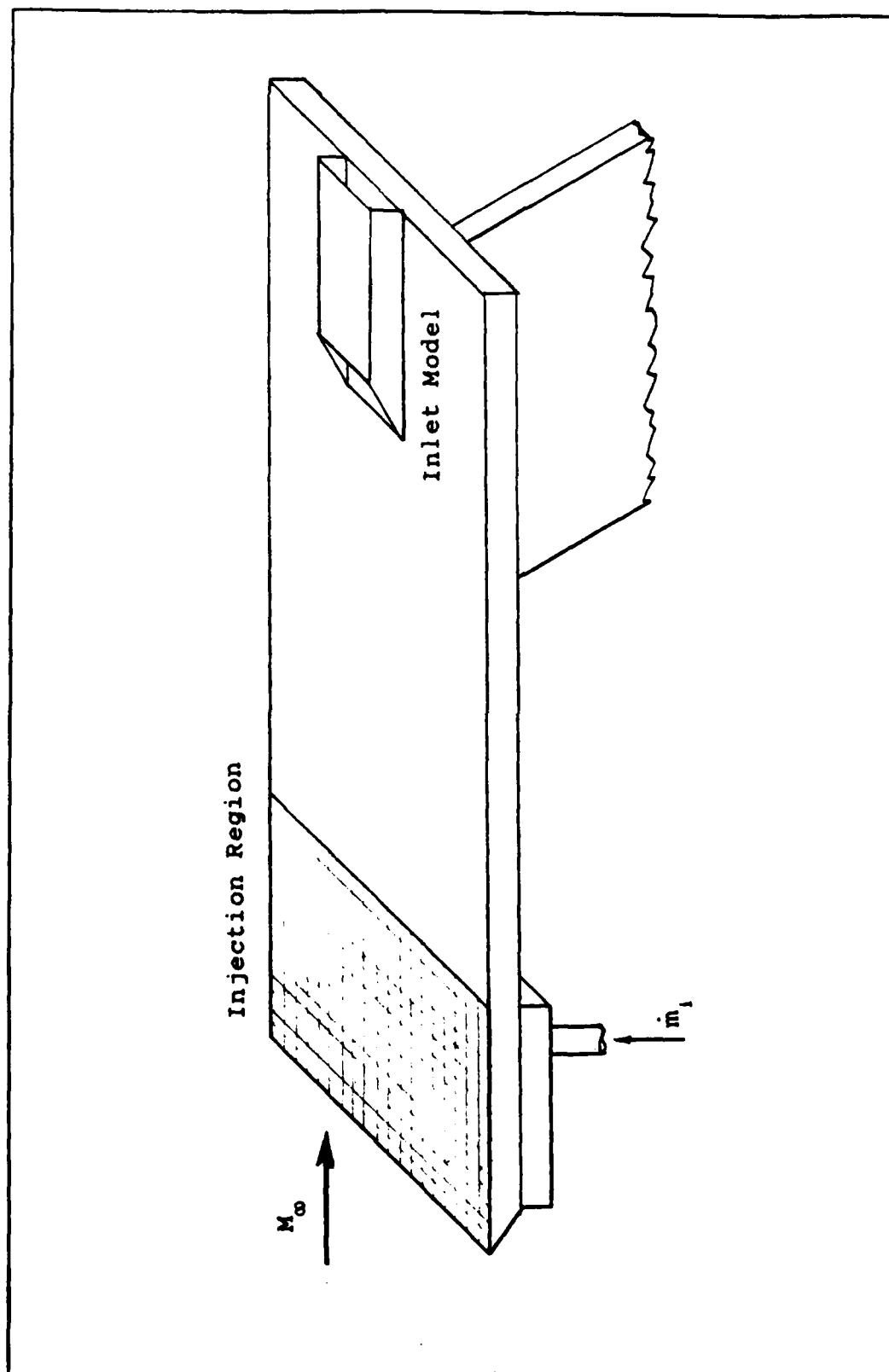
Fig. 3 Boundary Layer Generator System Schematic
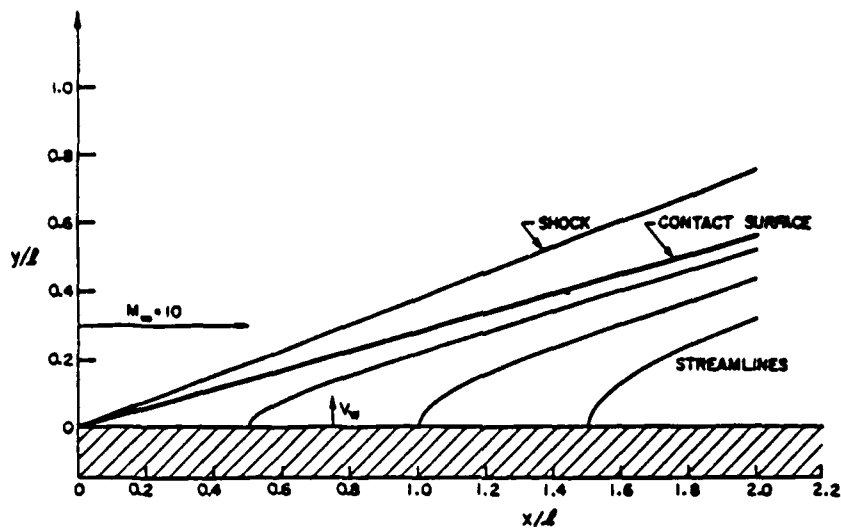
Fig. 4
Streamline Pattern for Constant Mass Injection from a Flat Plate
in Supersonic Flow $\theta_w = 0^o$, $\alpha = 16^o$

(Wallace and Kemp I, 1967:35)
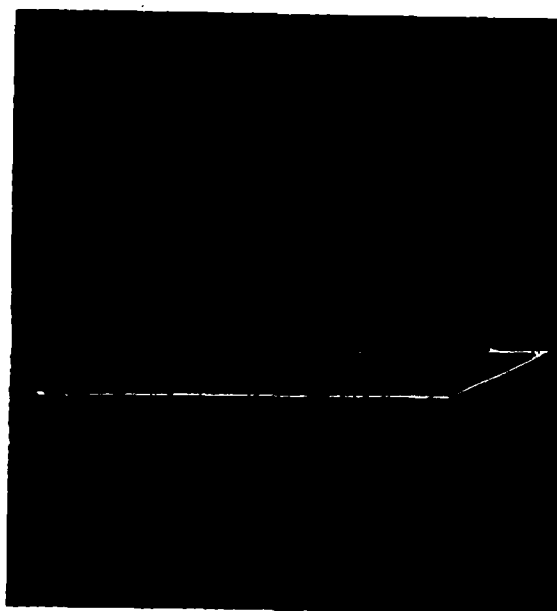
Fig. 5   Uniformly porous flat plate
Separation streamline visualization.

(Hartunian and Spencer,1966:1306)

35
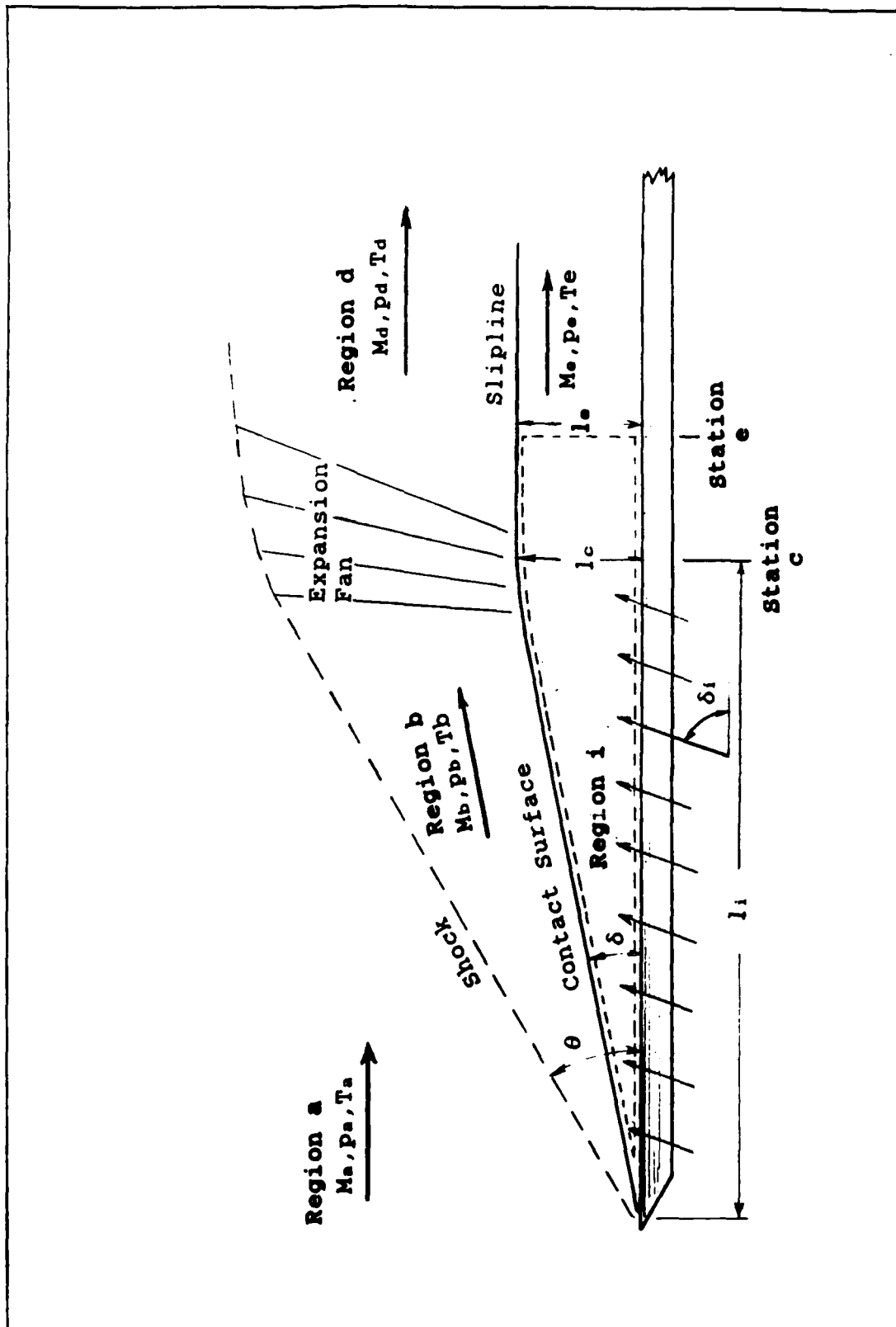
Fig. 6 Injection Region Flowfield Geometry.

Table 1: Mach 2.6 Results

Ma= 2.60   pa= 103.3   Ta= 229.6
Ti= 540.0   deltai= 90.00   li= .28

lambda	delta (deg)	pi (psf)	Ui (ft/s)	pd (psf)	Ue (ft/s)	Me	Te (R)	mdoti (slug/s)
.005	2.88	125.5	18.7	103.5	437.3	.39	523.6	.00072
.010	4.47	139.2	33.7	103.3	553.9	.50	514.4	.00143
.015	5.76	151.1	46.6	103.4	634.0	.57	506.7	.00215
.020	6.87	162.1	57.9	103.6	696.5	.64	499.9	.00287
.025	7.86	172.4	68.1	103.9	748.1	.69	493.8	.00358
.030	8.76	182.1	77.3	103.4	797.8	.74	487.3	.00430
.035	9.59	191.5	85.8	103.5	838.8	.78	482.0	.00502
.040	10.36	200.5	93.6	103.6	875.6	.82	476.9	.00573
.045	11.09	209.3	100.9	103.7	908.9	.85	472.0	.00645
.050	11.77	217.9	107.7	103.8	939.4	.89	467.3	.00717
.055	12.42	226.2	114.1	103.9	967.7	.92	463.1	.00788
.060	13.04	234.3	120.2	104.0	993.7	.95	458.8	.00860
.065	13.63	242.3	125.9	104.1	1018.3	.97	455.0	.00932
.070	14.19	250.1	131.4	104.3	1041.1	1.00	451.2	.01004
.075	14.73	257.8	136.6	104.4	1062.5	1.02	447.6	.01075

Fig. 7 Delta, Ui, pi and pb VS
Injected Mass Flow Parameter

Ma=2.6
pa=103.3 psf
Ta=229.6 R
Ti=540.0 R
li= 3.4 in
deltai= 90 deg

U̇i (ft/s), pi (psf)

delta (deg)

lambda infinity
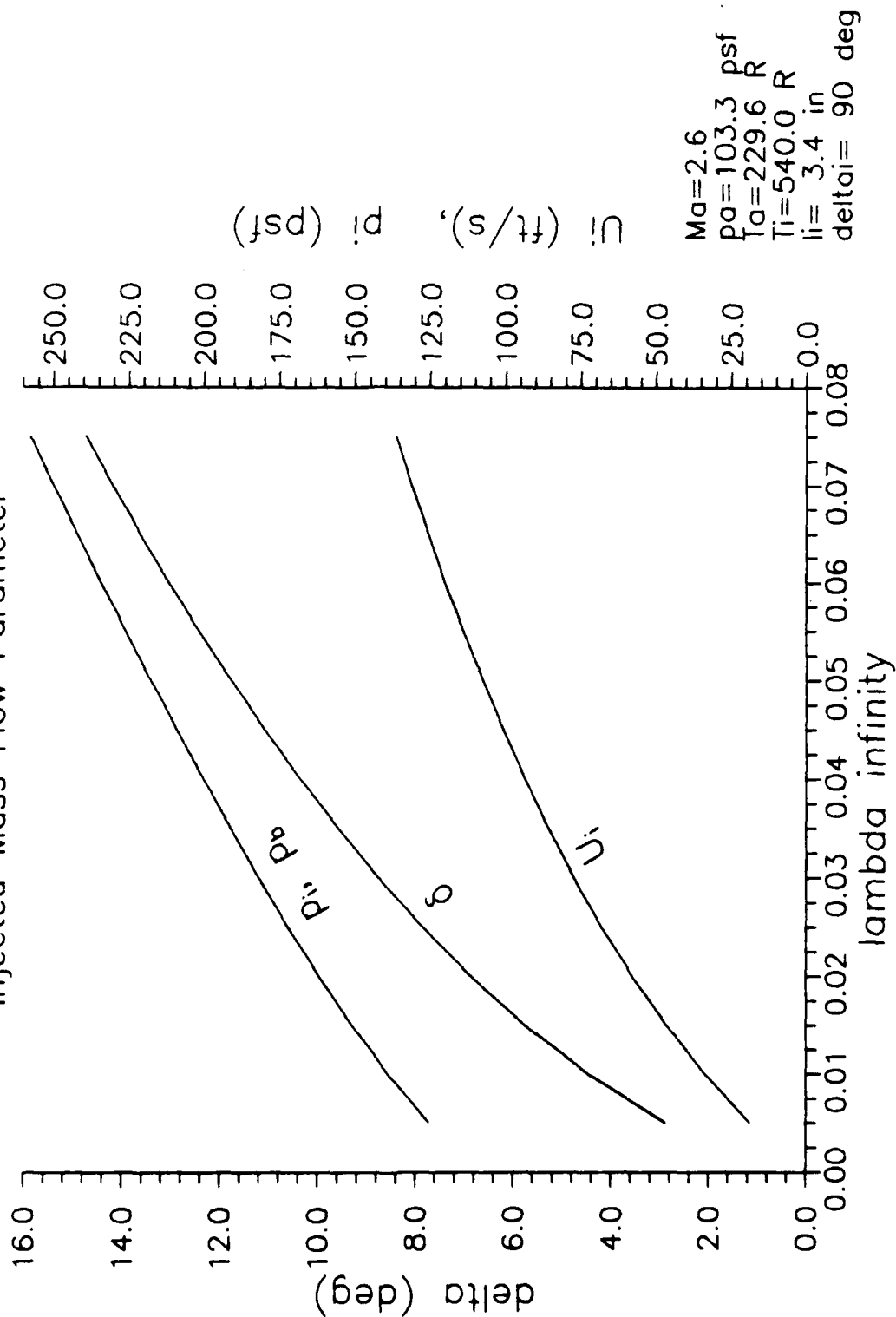
Fig. 8 Me, Te, pe and pd
Versus Lambda

Ma=2.6
pa=103.3 psf
Ta=229.6 R
Ti=540.0 R
li= 3.4 in
deltai= 90 deg

39
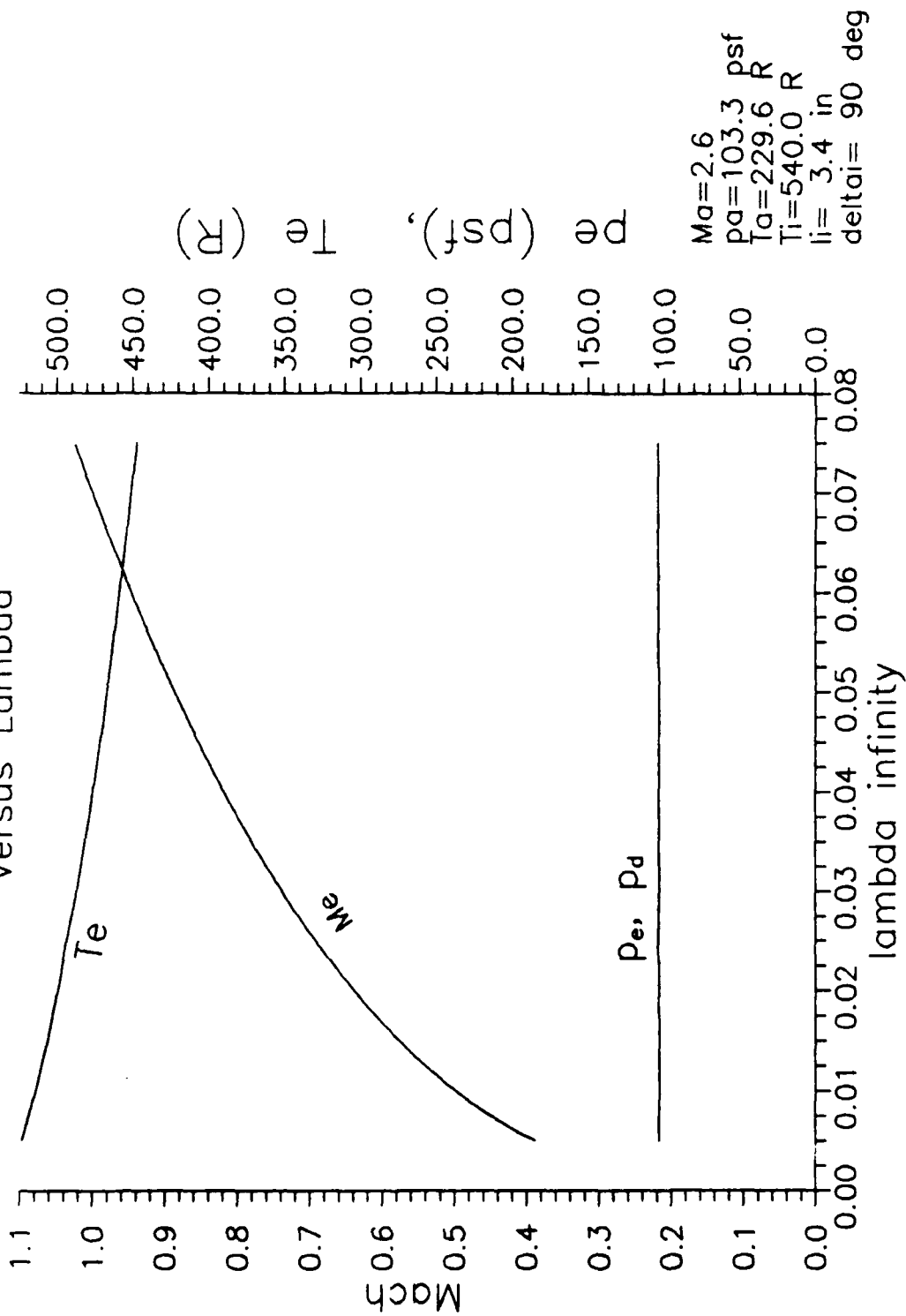
Fig. 9   CONTACT SURFACE DEFLECTION ANGLE
VS INJECTED MASS FLOW PARAMETER
10% le Variation

Ma=2.6
pa=209.4 psf
Ta=229.6 R

Ti=540.0 R
li= .283 ft
deltai= 90 deg

Experiment (Zukoski)
Calculated le= 0.9*li*tanδ
Calculated le= li*tanδ
Calculated le= 1.1*li*tanδ

delta

lambda infinity
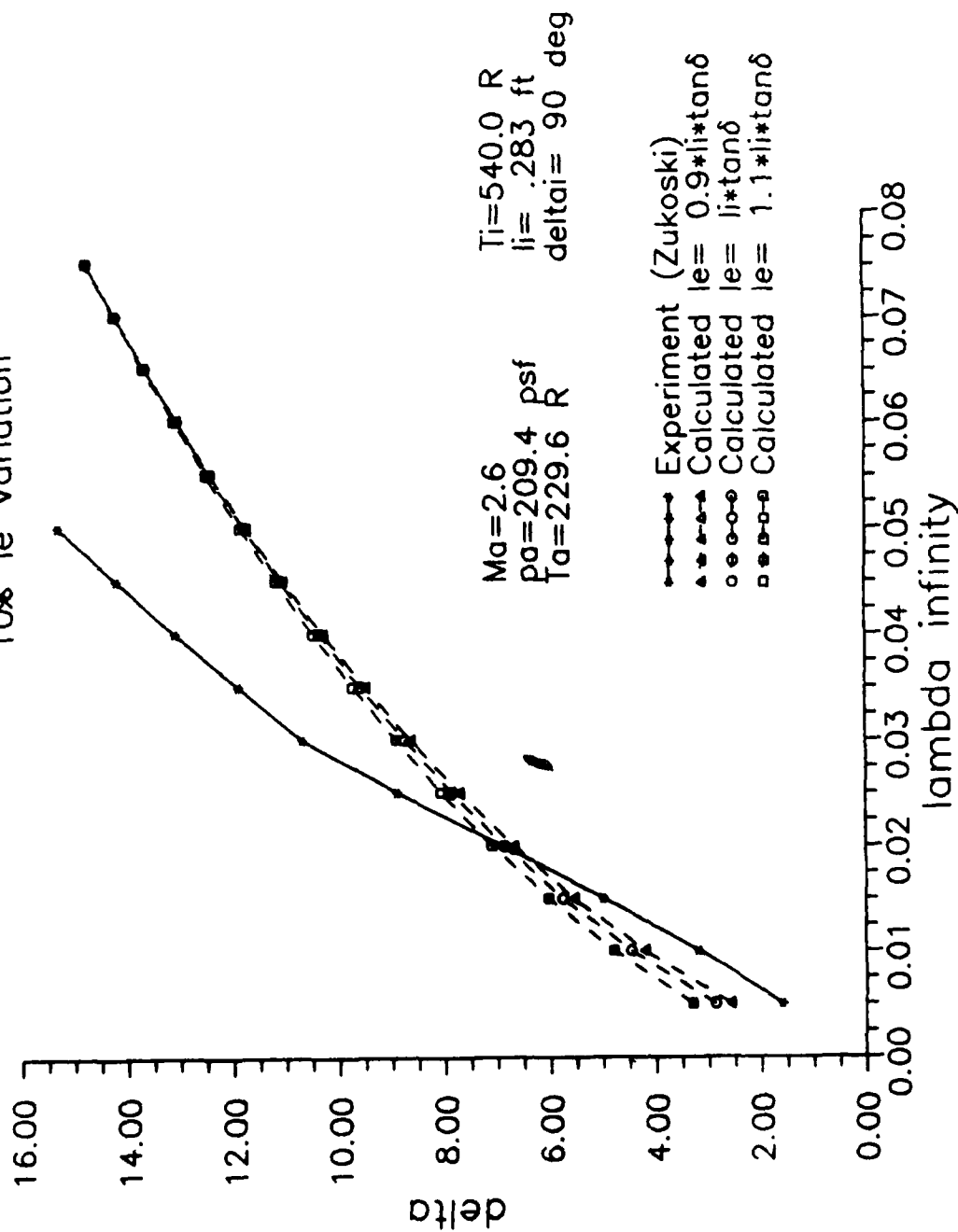
Fig. 10 CONTACT SURFACE DEFLECTION ANGLE
VS INJECTED MASS FLOW PARAMETER
10% Ma Variation

Ma=2.6   Ti=540.0 R
pa=103.3 psf   li= .283 ft
Ta=229.6 R   deltai= 90 deg

Experimental
Ma= 2.34
Ma= 2.60
Ma= 2.86

delta

lambda infinity
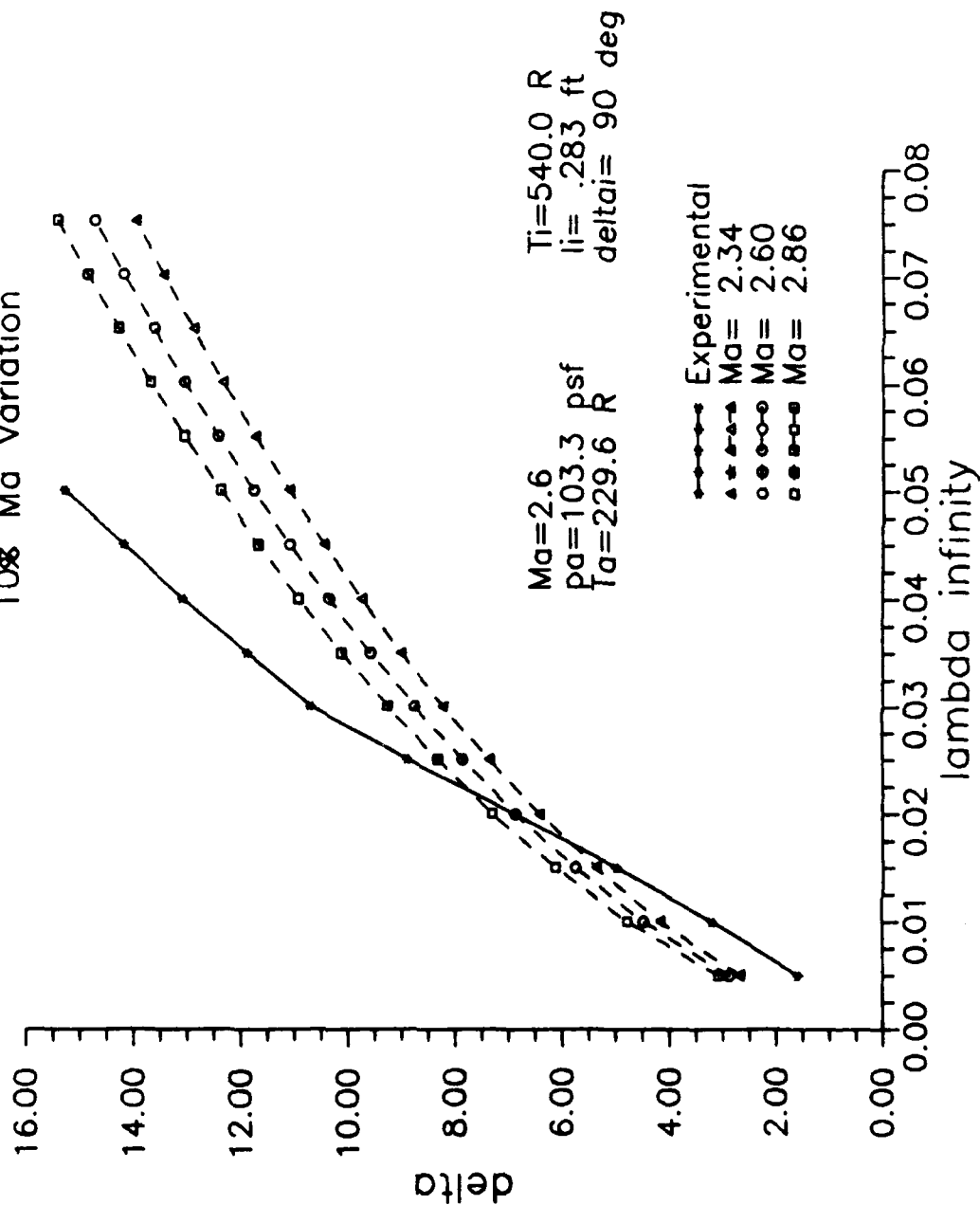
Fig. 11   CONTACT SURFACE DEFLECTION ANGLE
VS INJECTED MASS FLOW PARAMETER
10% Ta Variation

Ma=2.6
pa=103.3 psf
Ta=229.6 R

Ti=540.0 R
li= .283 ft
deltai= 90 deg

Experimental
Ta= 206 R
Ta= 229 R
Ta= 252 R

lambda infinity

delta
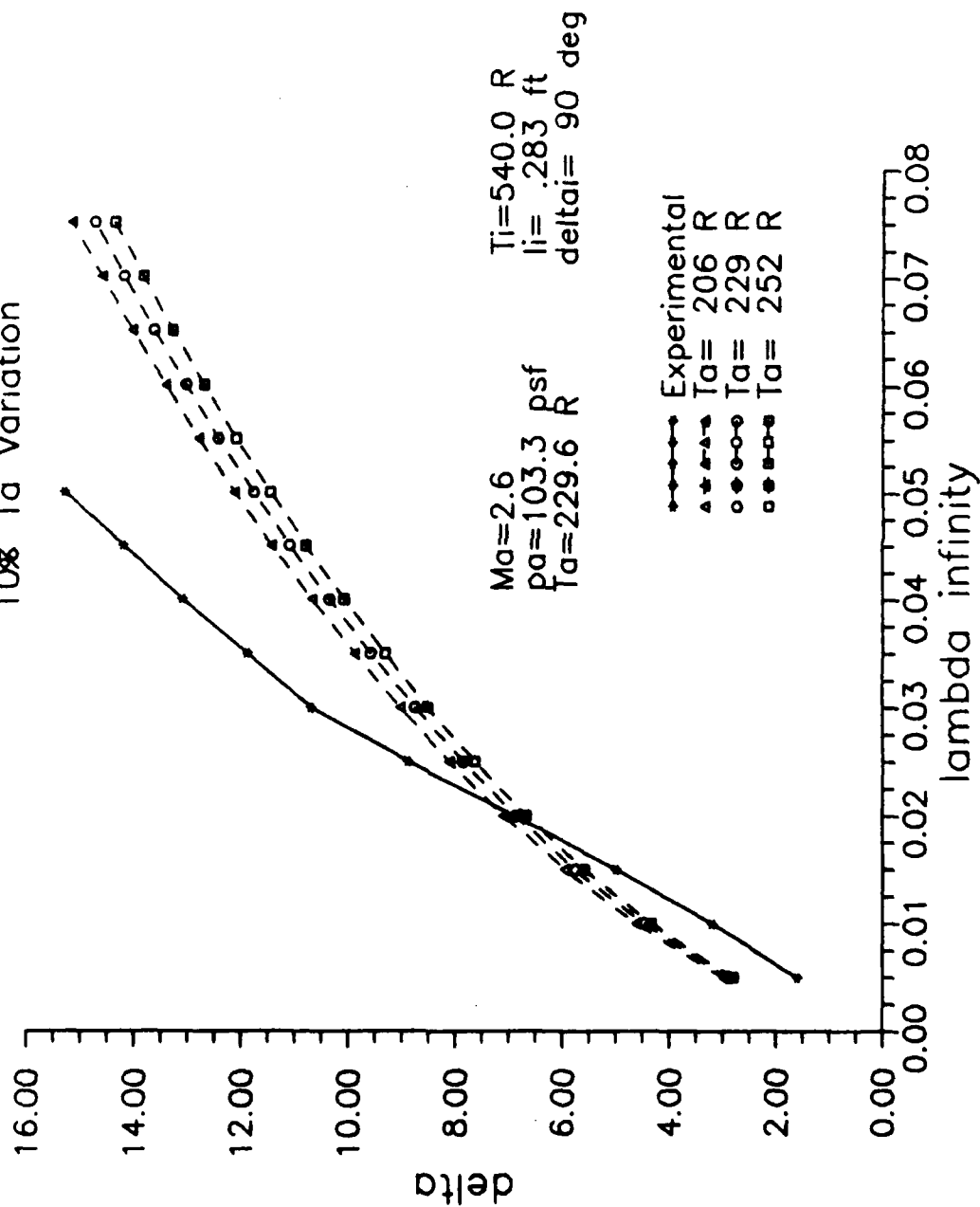
Fig. 12 CONTACT SURFACE DEFLECTION ANGLE VS INJECTED MASS FLOW PARAMETER 10% pa Variation

Ma=2.6
pa=103.3 psf
Ta=229.6 R

Ti=540.0 R
li= .283 ft
deltai= 90 deg

Experimental
pa= 93 psf
pa= 103 psf
pa= 113 psf

lambda infinity

delta

16.00
14.00
12.00
10.00
8.00
6.00
4.00
2.00
0.00

0.00 0.01 0.02 0.03 0.04 0.05 0.06 0.07 0.08
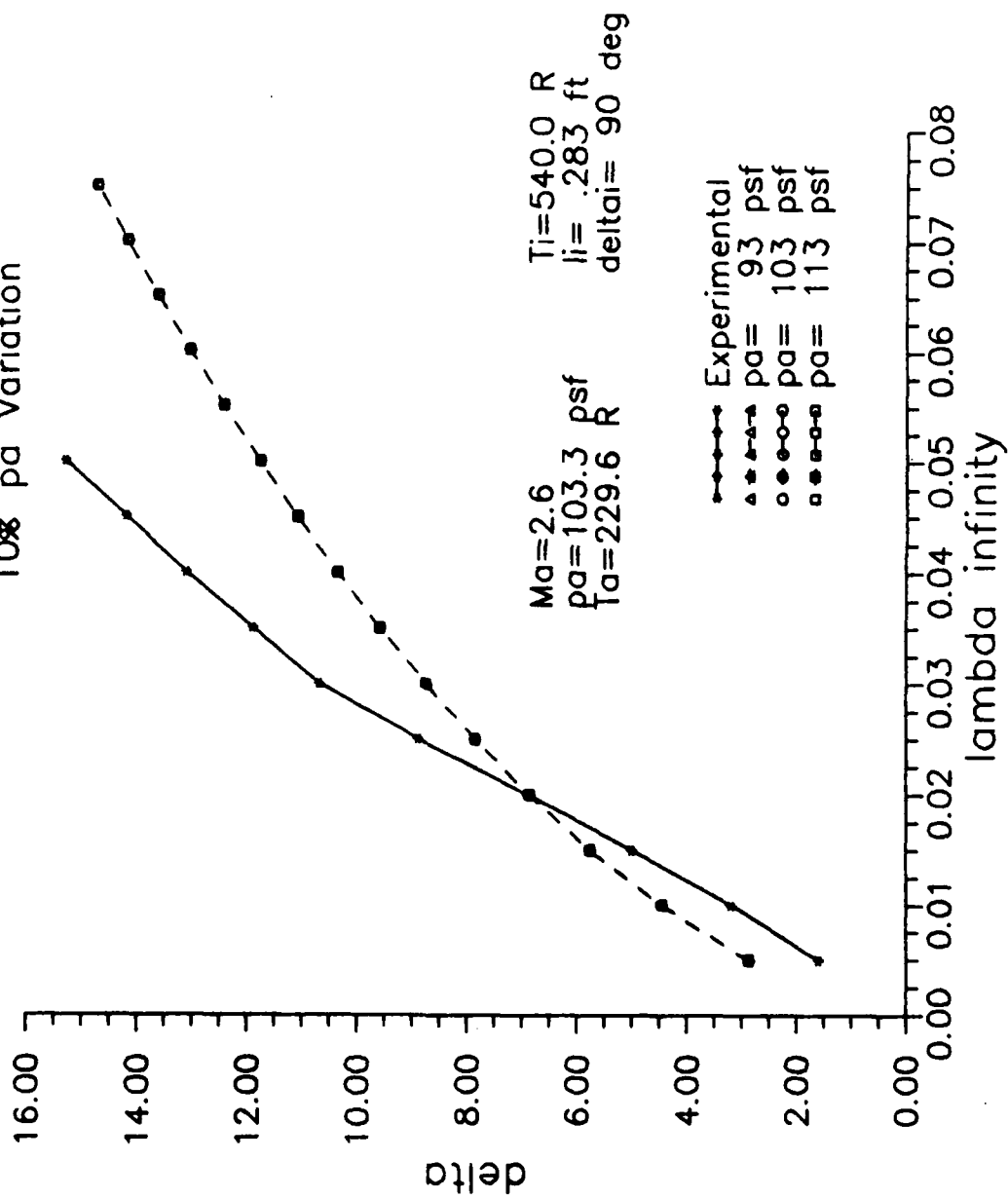
Fig. 13   CONTACT SURFACE DEFLECTION ANGLE
VS INJECTED MASS FLOW PARAMETER
10% Ti Variation
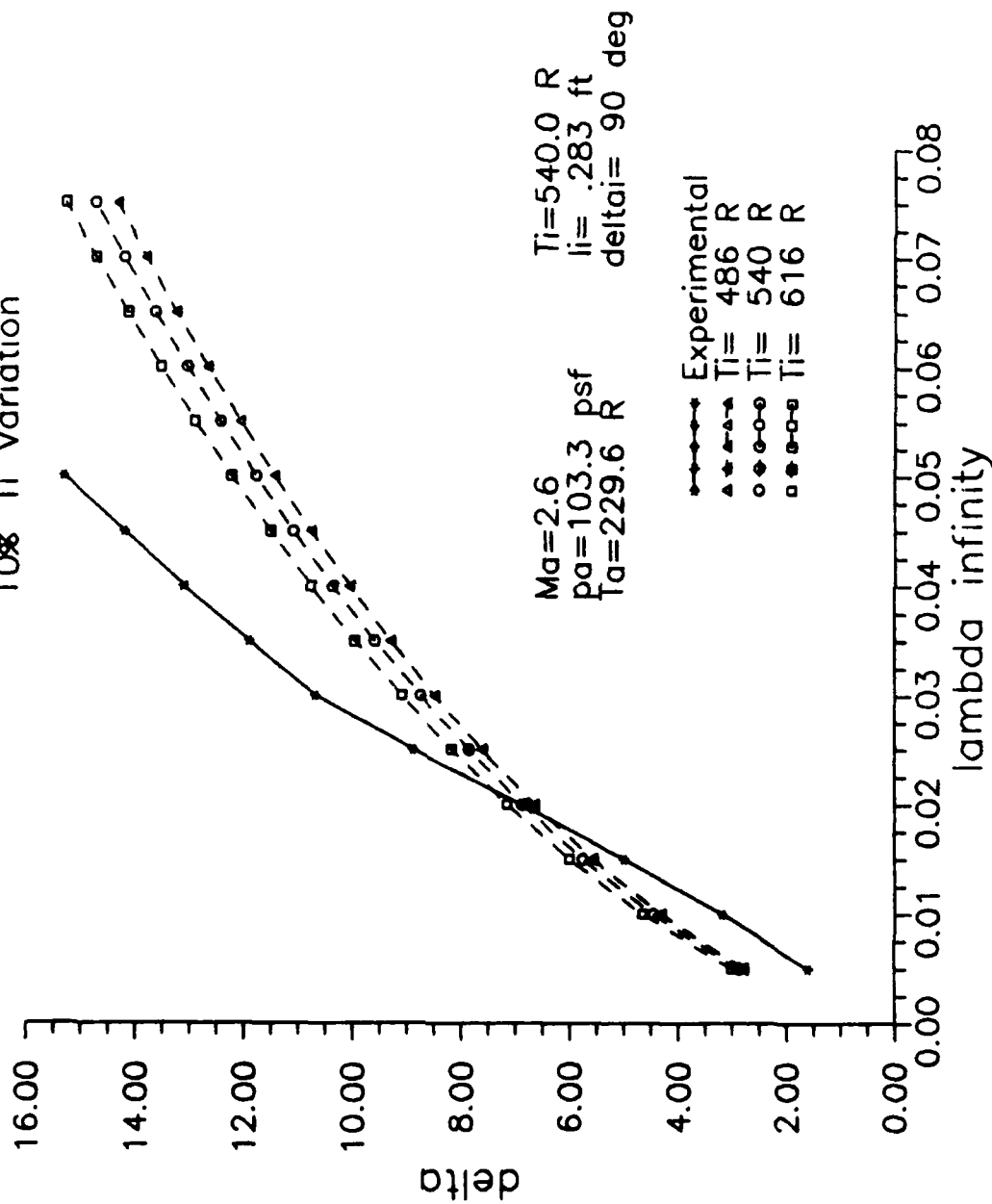
Ma=2.6
pa=103.3 psf
Ta=229.6 R

Ti=540.0 R
Ii= .283 ft
deltai= 90 deg

Experimental
Ti= 486 R
Ti= 540 R
Ti= 616 R

lambda infinity

delta

16.00   14.00   12.00   10.00   8.00   6.00   4.00   2.00   0.00

0.00   0.01   0.02   0.03   0.04   0.05   0.06   0.07   0.08

44

Fig. 14 CONTACT SURFACE DEFLECTION ANGLE
VS INJECTED MASS FLOW PARAMETER
10% δ_i Variation

Ma=2.6
pa=103.3 psf
Ta=229.6 R

Ti=540.0 R
li= .283 ft
deltai= 90 deg

Experimental
deltai= 81
deltai= 90
deltai= 99

lambda infinity

delta

45
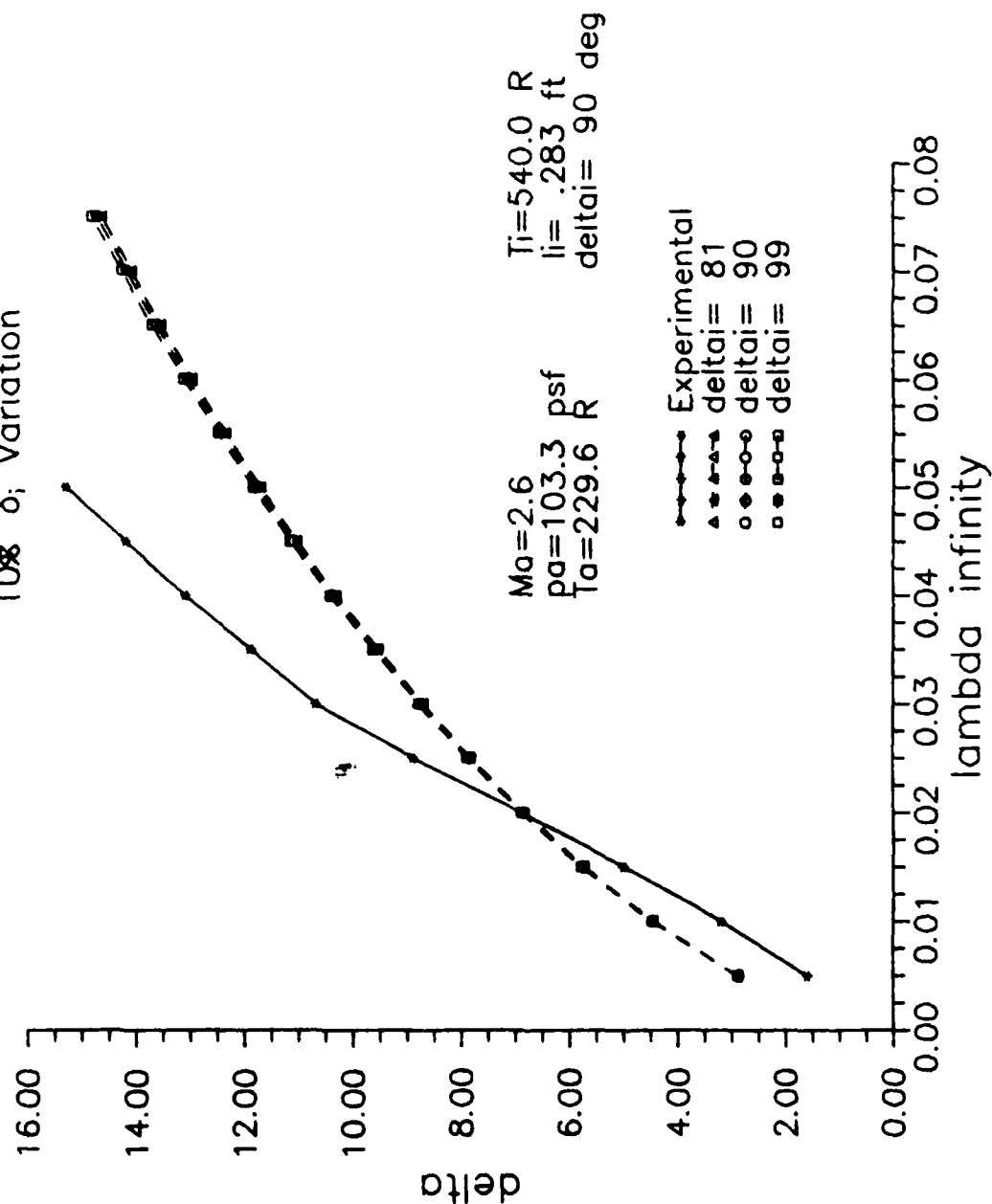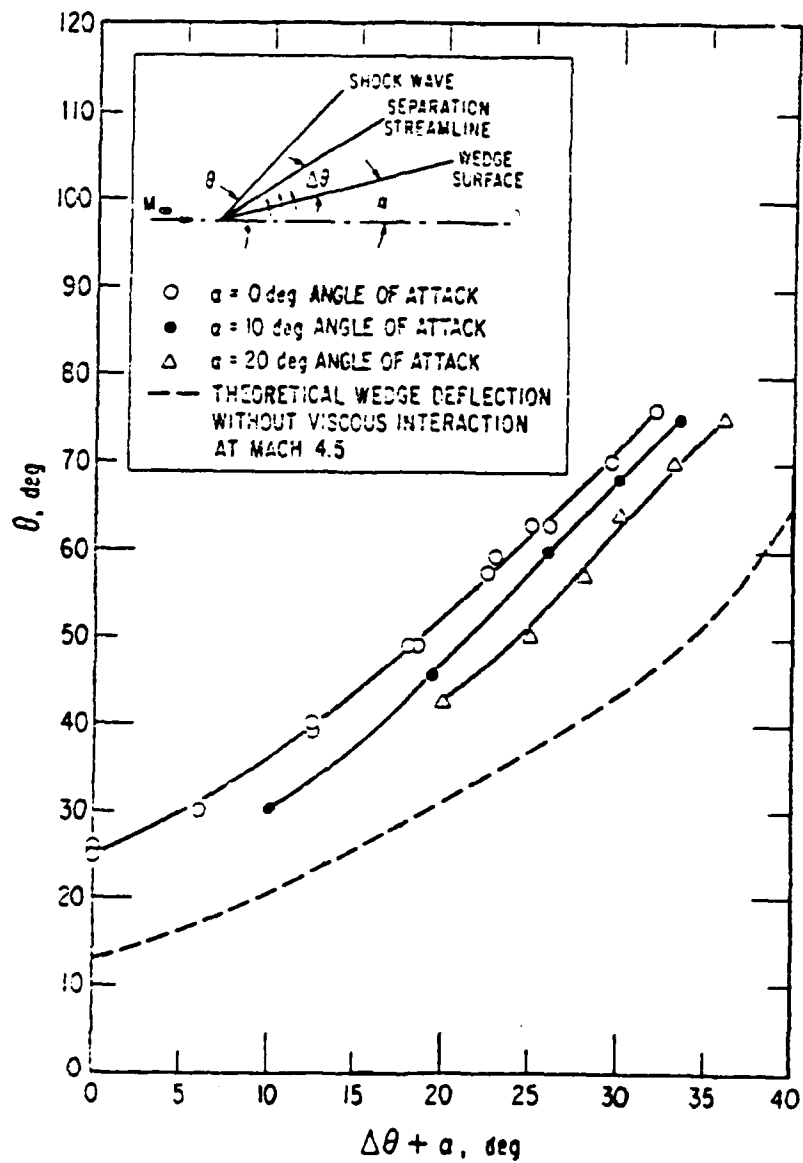
Fig. 15   Shock Angle Versus Contact Surface Deflection Angle   (Bott,1967:13)

46

Fig. 16 VELOCITY PROFILE
Example of the 'f' function
and 3rd Order Polynomial
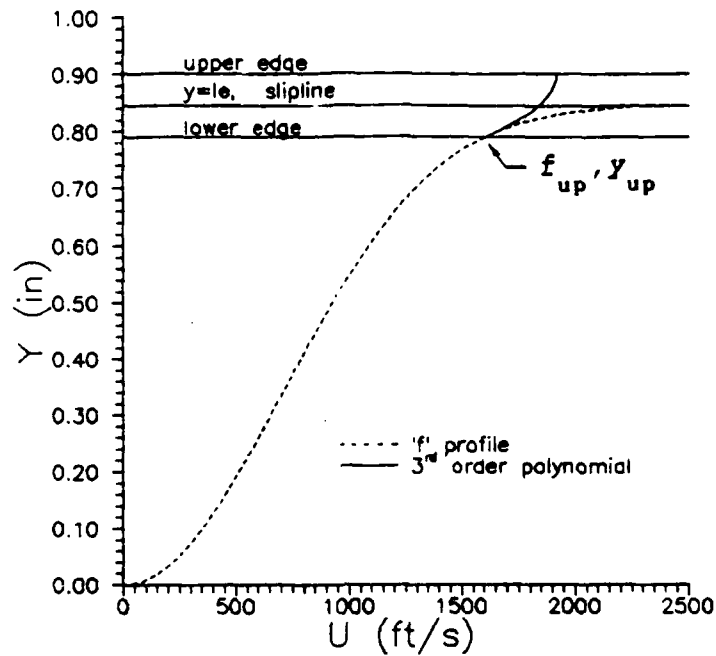
Fig. 17 TEMPERATURE PROFILE
Example of the 'f' function
and 3rd Order Polynomial

47
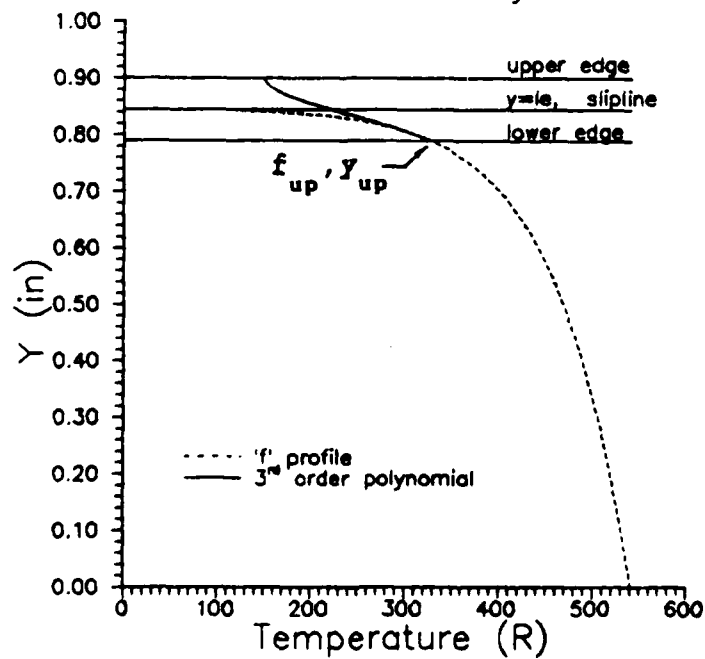
Fig. 18 Velocity Profiles
Aft of Injection Region
Mach= 4.38

x/l₀

18

12

6

0

Initial Profile:
Dashed: 'f' Function
Solid: Uniform

Squares indicate displacement
thickness for each profile.

U(ft/s)

Y(in)

48
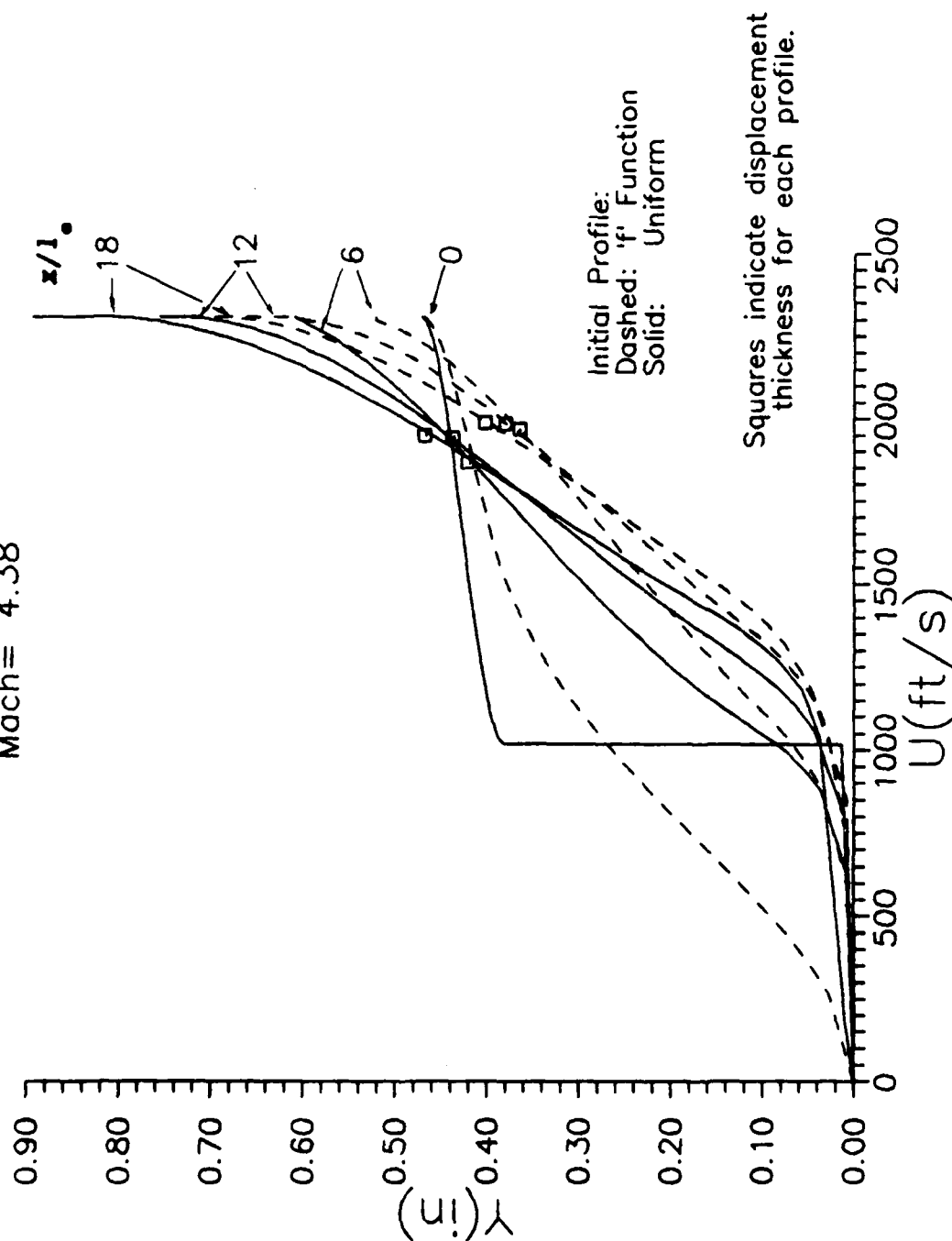
Fig. 19   Velocity Profiles
11 inches Downstream
Mach= 4.38

δ_{99}

λ = constant
= 0.0153

σ = .03
σ = .05
σ = .07

U(ft/s)

Y(in)

Boundary Layer Rakes

Injected Air Plenum
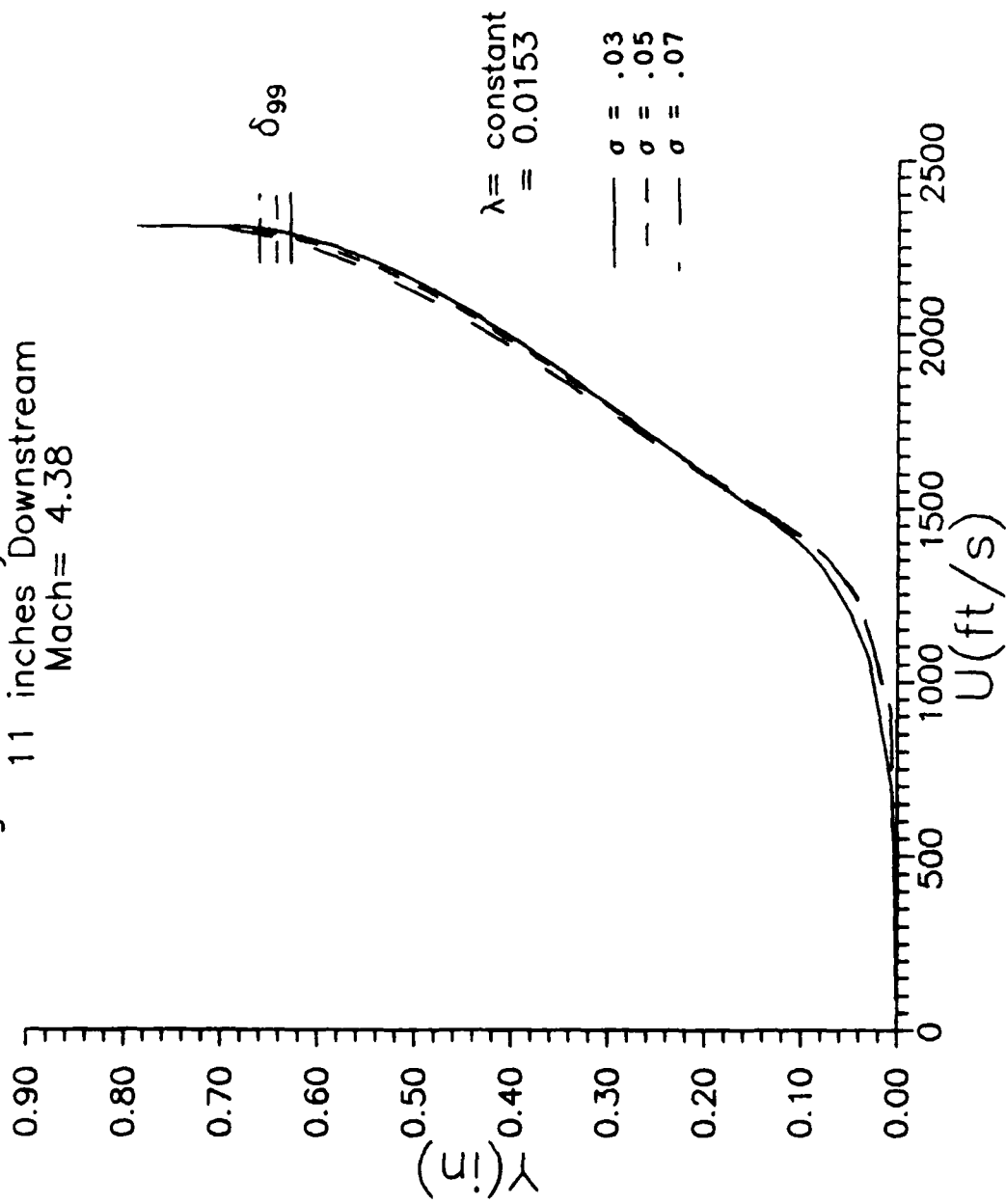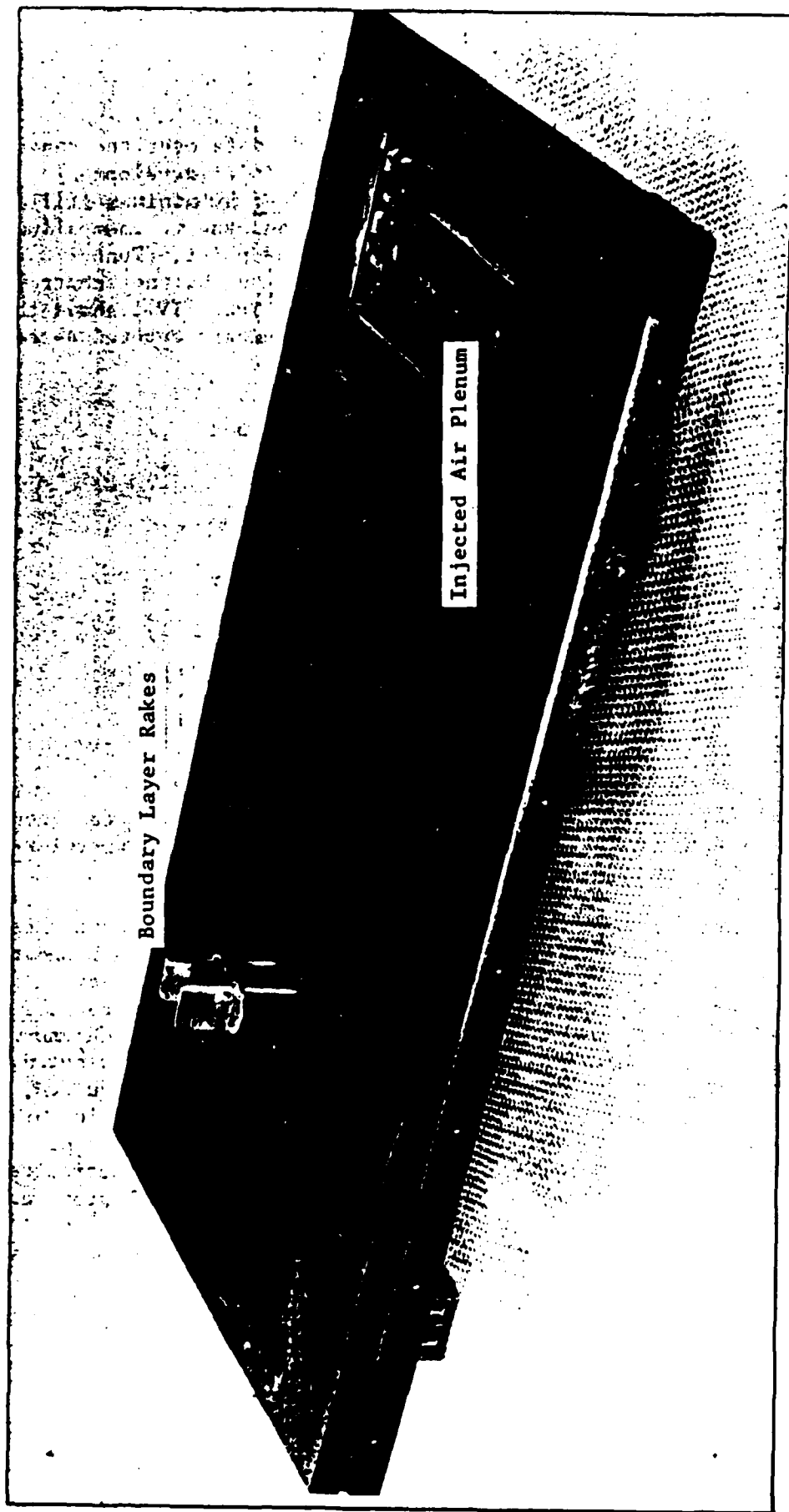
Fig. 20   Injection Hardware for Academy Test,
Mach=4.38 (Rozycki,1968:IV-3)

50
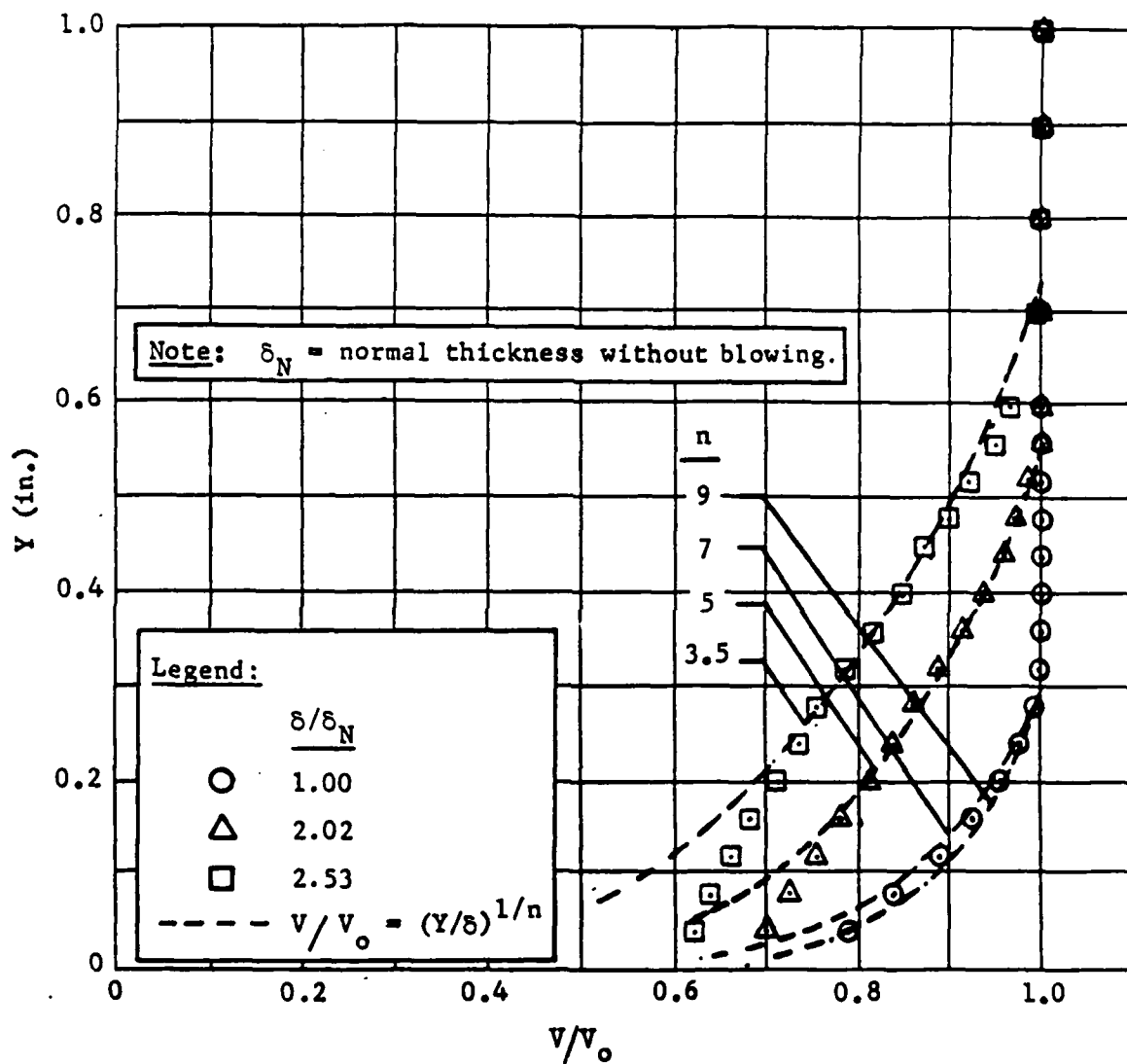
Fig. 21 Boundary Profiles for Academy Test, Mach=4.38 (Rozycki,1968:IV-16)

Fig. 22 Velocity Profiles 11 Inches
Aft of Injection Region
Ma= 4.38

δ_{99}=.627

δ_{99}=.508

δ_{99}= .627 'f' initial profile
uniform initial profile
expermental results
δ_{99}= .508 'f' initial profile
uniform initial profile
expermental results

λ was varied for the 'f'
profile until δ_{99} matched the
test data. λ was held at that
value for the uniform profile.

Ue (ft/s)

Y (in)
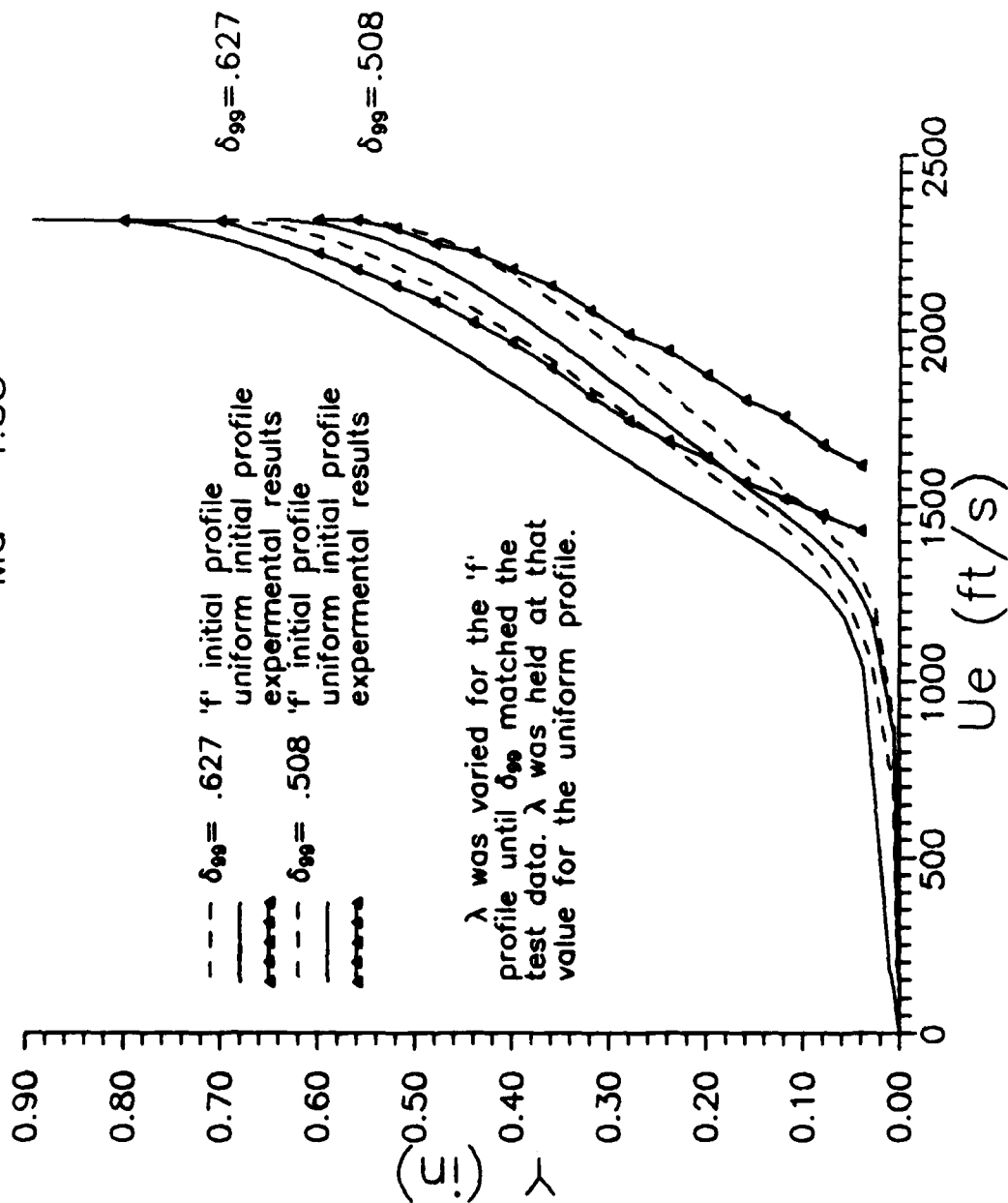
Fig. 23 Velocity Profiles
Mach 10, Nitrogen
xl= 6 ft

— Injection Profile
– – 1/7 Power Law

li= 2.0 ft

li= 1.0 ft

li= 0.5 ft

6 ft δ_{99} WITHOUT BLOWING
(See Introduction)

U (ft/s)

Y (in)

10.00
9.00
8.00
7.00
6.00
5.00
4.00
3.00
2.00
1.00
0.00

0
1000
2000
3000
4000
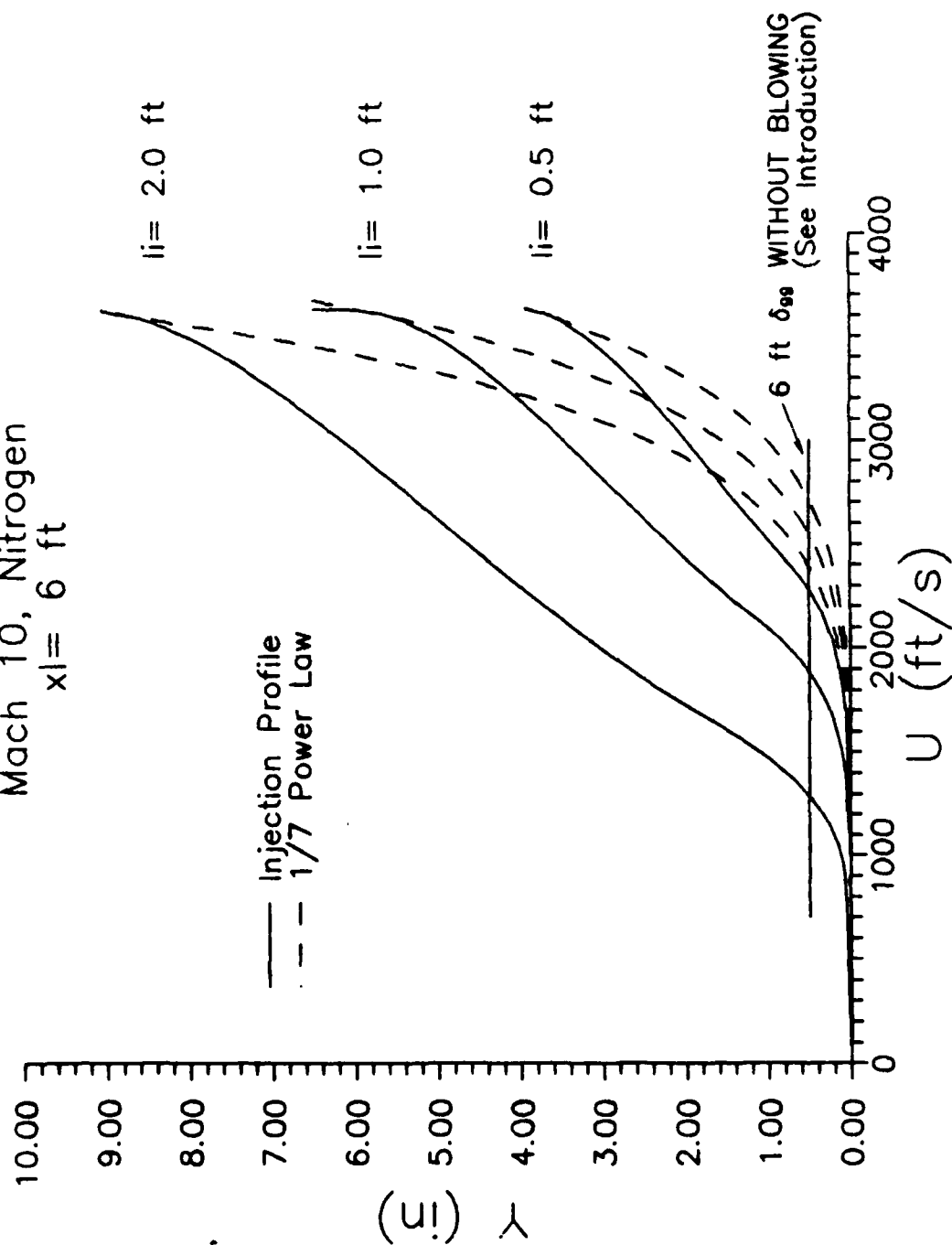
Fig. 24   Temperature Profiles
Mach 10, Nitrogen
xl= 6 ft

li= 2.0 ft

1.0 ft

0.5 ft

Temperature (R)

Y (in)

54
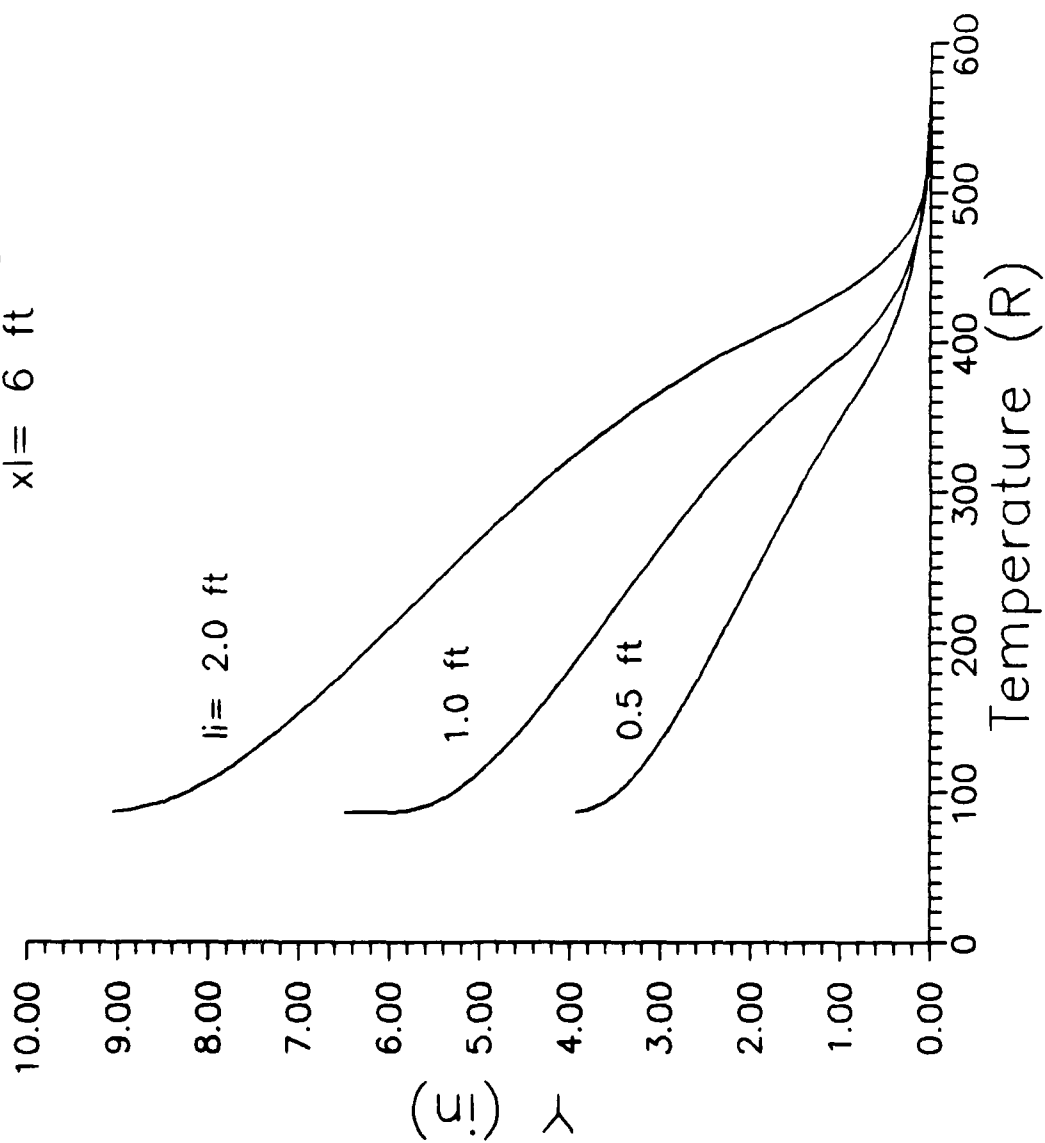
Appendix A

Flowchart for INJECT.FOR

```
Start
  │
Read Input
  │
guess θ
  │
CALL MDDIFF to          ◄───────────────┐
calculate ṁₑ                            │
  │                                      │
ṁₑ=ṁᵢ ──N──►  revise θ
  │           Newton-Raphson
  Y
  │
calculate Re
  at e
  │
calculate δ
w/o blowing
for comparison
  │
guess Vw
  │
CALL MDEDIFF
to calculate profile    ◄───────────────┐
at e and integrate                       │
profile for ṁ                            │
  │                                      │
ṁ=ṁₑ ──N──►  revise Vw
  │          Newton-Raphson
  Y
  │
calculate y+
  │
Write file PROFILE
for TEXSTAN input
  │
calulate momentum and
energy by integrating
profiles
```

```
          │
CALL INPUTD to
set up TEXSTAN
input file
          │
     CALL TEXTAN
          │
        STOP
```

55

```
*****************************************************************************
*                                                                           *
*                              INJECT.FOR                                   *
*                                                                           *
*                           Capt Robert Clausen                             *
*                      Air Force Institute of Technology                    *
*                                                                           *
*        INJECT.FOR is a Fortran program which models mass addition (blowing) *
*  on a flat plate into a supersonic stream.  This program calls the boundary *
*  layer code TEXSTAN (Kays and Crawford) to then calculate boundary layer  *
*  development aft of the injection region.  In order to understand the      *
*  injection phenomena and analysis method of this code, please obtain a     *
*  copy of the AFIT Thesis 'A Computational Model For Thickening Boundary     *
*  Layers With Mass Addition for Hypersonic Engine Inlet Testing'.           *
*                                                                           *
*****************************************************************************
      PROGRAM INJECT
      Implicit Real*8 (a-h,m,l,o-z)
      Character*72 filenm,title
      grekpi= 3.141592654
c
c-- Open input file 'injs.inp' and output file ---
c
      OPEN (3,file='inject.inp',status='old')
      Read(3,406)filenm,gamma,Cp,R, Ma,pta,Tta,Ti,li,deltid,lambda,
     $ xl,slipfr,title
  406 Format(1x,///,13x,A14,/,12(13x,f10.0,/),/,A72)
      OPEN (6,file=filenm,status='unknown')
      Write(6,458)title
  458 Format(A72,//)

      Ta=Tta/(1.0+(gamma-1.0)/2.0*Ma*Ma)
      pa= pta/(1.0+(gamma-1.0)/2.0*Ma*Ma)**(gamma/(gamma-1.0))
      deltai= deltid * grekpi/180.0
      mdoti= lambda*(pa/R/Ta*Ma*DSQRT(gamma*R*Ta))*li


c
c-- Determine Mach wave angle (thetam) as a function of freestream Mach --
c     and use it for the initial guess for the iteration.
c
      thetaMW= DASIN(1.0/Ma)
      theta= thetaMW + 10.0*grekpi/180.0
c
c--- Iterate on theta using a Newton-Raphson method until mdote=mdoti -----
c
      iter=0
      dtheta=0.02*grekpi/180.0
   10 CALL MDDIFF(mddifnom, theta,Ma,pa, Ti,li,mdoti,deltai,
     $ gamma,Cp,R, pe,Ue,Te, pi,Ui,pd,Me,delta,Md)
      IF (DABS(mddifnom) .LE. (mdoti/1000.0)) GO TO 11
```

```fortran
         iter= iter+1
         IF (iter .GT. 25) GO TO 12
         CALL MDDIFF(mddifr, theta+dtheta,Ma,pa, Ti,li,mdoti,deltai,
      $  gamma,Cp,R, pe,Ue,Te, pi,Ui,pd,Me,delta,Md)
         CALL MDDIFF(mddifl, theta-dtheta,Ma,pa, Ti,li,mdoti,deltai,
      $  gamma,Cp,R, pe,Ue,Te, pi,Ui,pd,Me,delta,Md)
         theta= theta- (2.0*dtheta*mddifnom)/(mddifr-mddifl)
         GO TO 10
   12 Write(6,407)iter-1,mddifnom
         Write(*,407)iter-1,mddifnom
  407 Format(' The number of iterations has exceeded',I2,'.',
      $ '    mdiff=',f10.1)
   11 Continue
c
c--- Write injection region output --------------
c
         Ua= Ma*DSQRT(gamma*R*Ta)
         Write(6,503)Ma,Ua,pa,pta,Ta,Tta
  503 Format(' Ma=',f5.2,2x,'Ua(ft/s)=',f6.1,2x'pa(psf)=',f6.1,2x,
      $ 'pta(psf)=',f10.1,2x,/,' Ta(R)=',f6.1,2x,'Tta(R)=',f6.1,/)
         Write(6,502)delta*57.296
  502 Format(' Contact surface ("wedge") angle delta(deg)=',f5.1,/)
         Write(6,504)mdoti,lambda,pi,Ui,Ti,deltid,li
  504 Format(' mdoti(slug/s)=',f7.5,2x,'lambda=',f6.4,2x,'pi(psf)=',
      $ f6.1,2x,'Ui(ft/s)=',f6.1,2x,/,'Ti(R)=',f6.1,2x,
      $ 'deltai(deg)='f5.1,2x,'li(ft)=',f6.4,/)
         Td= Tta/(1.0+(gamma-1.0)/2.0*Md*Md)
         Ud= Md*DSQRT(gamma*R*Td)
         ptd= pd*(Tta/Td)**(gamma/(gamma-1.0))
         Write(6,505)Md,Ud,pd,ptd,Td,Tta
  505 Format(' Md=',f5.2,2x,'Ud(ft/s)=',f6.1,2x,'pd(psf)=',f6.1,2x,
      $ 'ptd(psf)=',f8.1,2x,/,' Td(R)=',f6.1,2x,'Ttd(R)=',f6.1,/)
         le= li*DTAN(delta)
         Write(6,506)Me,Ue,pe,Te,le
  506 Format(' Me=',f5.2,2x,'Ue(ft/s)=',f6.1,2x,'pe(psf)=',f6.1,2x,
      $ 'Te(R)=',f6.1,2x,/,'le(ft)=',f6.4,/)
c
c--- Calculate the Reynolds number at station e -----
c
         Re= ud*(li+le)/visc(Td,pd)
         Write(6,507)Re
  507 Format(' Reynolds Nu. at Station E =',e10.4,/)
c
c--- Calculate the boundary layer thickness at these conditions on a plate ---
c      of the same length for comparison.
c
         del99= 0.37 * xl * (1.0d0/(Ua*xl/visc(Ta,pa)))**.2
         del1= del99/8.0
         del2= del99 *7.0/72.0
         Write(6,508)xl,del99*12.,del1*12.,del2*12.
  508 Format(' Boundary layer thicknesses at xl(ft)=',f5.2,' without
      $injection',/,' delta99(in)=',f7.4,4x,
      $ 'displacement delta1(in)=',f7.4,4x,'momentum delta2(in)=',f7.4,/)
```

```
c
c--- Determine fup from slipstream thickness ---
c
      c= grekpi/2.0/delta/delta
      IF(DSIN(delta) .GT. slipfr/2.0) GO TO 26
      Write(*,421) delta*57.3
  421 Format(' delta= ',f5.2,'which causes the slipstream to occupy',
     $ ' the entire region "e".',/,
     $ ' Increase the injected mass flow (lambda).')
      STOP
   26 fup= slipfr/2.0/DSIN(delta)
      hti= Cp*Ti + Ui**2/2.0
c
c--- Find the 'f' profile which yields conservation of mass at station e. ---
c        Iterate on u at fup (uup) until the massflow calculated from
c        integrating the 'f' profile and slipstream profile equals mdote.
c        A Newton-Raphson iterative skeme is used.
c
      duup= 0.0001*ud
      uup= 0.84*ud
   27 Teup= (hti - uup**2/2.0)/Cp
      IF (Teup .GE. 0.0) Go To 28
      uup= 0.89*uup
      Go To 27
   28 CALL MDEDFF(mdenom,uup,fup,ud,Td,c,le,hti,mdoti,Cp,R,pe,
     $ au,bu,cu,du, aT,bT,cT,dT, Vw)
      IF(DABS(mdenom) .LE. (mdoti/1000.0))GO TO 31
      CALL MDEDFF(mder,uup+duup,fup,ud,Td,c,le,hti,mdoti,Cp,R,pe,
     $ au,bu,cu,du, aT,bT,cT,dT, Vw)
      CALL MDEDFF(mdel,uup-duup,fup,ud,Td,c,le,hti,mdoti,Cp,R,pe,
     $ au,bu,cu,du, aT,bT,cT,dT, Vw)
      uup= uup - (2.0*duup*mdenom)/(mder-mdel)
      GO TO 27
c
c--- Determine y at the edge of the law-of-the-wall region so that this option
c        can be used in TEXSTAN. A Newton-Raphson iterative method is used.
c
   31 yup= le*(1.0-fup)
      yd= le*(1.0+fup)
      ylawwa= 0.05*yup
      dylaw= 0.0001*yup
      viscw=visc(Ti,pe)
   43 ylawnom= YLAWDF(ylawwa,Vw,le,c,viscw)
      IF(DABS(ylawnom) .LE. 0.1) GO TO 44
      ylawwa= ylawwa-(2.0*dylaw*ylawnom)/
     $ (YLAWDF(ylawwa+dylaw,Vw,le,c,viscw)-
     $ YLAWDF(ylawwa-dylaw,Vw,le,c,viscw))
      GO TO 43
c
c--- Write the velocity profiles to file 'PROFILE' for input into Texstan ---
c        y in ft, Velocity in ft/s, Static entha   in BTU/lbm.
c
   44 OPEN(5,file='PROFILE',status='unknown')
```

```fortran
      write(5,479)title
  479 Format(A64)
      y0= 0.0d0
      u0= 0.0d0
      Write(5,427)y0,u0,Cp*Ti/778.0/32.2
  427 Format(3(e10.4))
c
c-- 'f' profile region --
c
      Nlower= 40
      dely=(yup-ylawwa)/DBLE(Nlower)
      Do 152 i=1,Nlower
      ai=i
      ye=ai*dely+ylawwa
      fe=1.0-ye/le
      uep= Vw*DSQRT(1.0-fe**2-2.0*c*DLOG(fe))
      he= (hti-Vw**2*(1.0-fe**2-2.0*c*DLOG(fe))/2.0)/778./32.2
  152 Write(5,427)ye,uep,he
c
c-- slipstream region --
c
      Nslip= 30
      dely=(yd-yup)/DBLE(Nslip)
      Do 153 i=1,Nslip
      ai= i
      ye= ai*dely+yup
      uep= au*ye**3 + bu*ye**2 + cu*ye + du
      he= (aT*ye**3 + bT*ye**2 + cT*ye + dT)*Cp/778./32.2
  153 Write(5,427) ye,uep,he
      N= Nlower + Nslip
      Rewind 5
      Close(5)
c
c--- Determine the momentum and energy of the fluid at station 'e' from
c       the 1-D properties and compare them to the momentum and enery
c       calculated by numerically integrating the 'f' velocity profile.
c       This serves as a check to determine how closely the assumed 'f'
c       profile conserves mass, momentum and energy.  (Note that the
c       assumed 'f' profile at 'e' was defined by conserving massflow).
c
c--- Calculate the momentum and enery from 1-D properties
c
      mom1D= pe/R/Te*Ue**2*le + pe*le
      E1D=   pe/R/Te*Ue*le*(Cp*Te + Ue**2/2.0)
c
c--- integrate the momentum and energy profile in region e
c--- integrate the region below the slipline
c
      df= (1.0-fup)/200.0
      sum1= 0.0
      sum8= 0.0
      Do 101 k=1,200
      ak= k
```

```fortran
      f= (ak-0.5)*df + fup
      ul= Vw*DSQRT(1.0 - f**2 -2.0*c*DLOG(f))
      sum1= sum1 + ul**2/(hti-ul**2/2.0)*df
  101 sum8= sum8 + ul *(1.0 + ul**2/2.0/(hti-ul**2/2.0))*df
      mom1= pe*le*Cp/R*sum1
      E1=   pe*le*Cp/R*sum8
c
c---  integrate the massflow in the slipline ----
c
      dy= (le-yup)/100.0
      sum2= 0.0
      sum9= 0.0
      Do 102 k=1,100
      ak= k
      y= (ak-0.5)*dy + yup
      us=  au*y**3 + bu*y**2 + cu*y + du
      Tes= aT*y**3 + bT*y**2 + cT*y + dT
      sum2= sum2 + us**2/Tes*dy
  102 sum9= sum9 + us*(Cp + us**2/2.0/Tes)*dy
      moms= pe/R*sum2
      Es=   pe/R*sum9

      mome= mom1 + moms + pe*le
      Ee=   E1 + Es
      perdfm= DABS(mom1D-mome)/mom1D
      perdfE= DABS(E1D-Ee)/E1D

      Write(6,466) mom1D,mome,perdfm*100.,E1D/778.,Ee/778.,perdfE*100.
  466 Format(' Momentum at Station ''e'''',/,' 1-D (lbf)=',f8.2,
     $ 5x,' ''f'' Profile (lbf)=',f8.2,5x,/,' percent difference =',f7.1,
     $ //,' Energy at Station ''e'''',/,' 1-D (Btu/s)=',f8.2,5x,
     $ ''f'' Profile (Btu/s)=',f8.2,5x,/,' percent difference=',f7.1,//)
c
c--- Set up the TEXSTAN input file -------------------------------------
c
      xu= li+le
      hw= Ti*Cp/778./32.2
      hd= Td*Cp/778./32.2
      CALL INPUTD(title,xu,xl,pd,ud,hw,hd,N)
c
c-- Start TEXSTAN --------------------
c
      CALL TEXSTAN

      STOP
      END
c
c**********************************************************************
c
      SUBROUTINE MDDIFF(mddif, theta,Ma,pa, Ti,li,mdoti,deltai,
     $ gamma,Cp,R, pe,Ue,Te, pi,Ui,pd,Me,delta,Md)
      Implicit Real*8 (a-h,m,l,o-z)
```

60

```fortran
      delta= DATAN(1.0/((gamma+1.0)*Ma*Ma/2.0/((Ma*DSIN(theta))**2-1.0)
     $ -1.0)/DTAN(theta))
      lc= li*DTAN(delta)
      pb= pa*(2.0*gamma*Ma*Ma*DSIN(theta)**2 - (gamma-1.0))/(gamma+1.0)
      pi= pb
      Ui= mdoti*R*Ti/pi/li
c
c-- Solve for the conditions in region 'd' after the expansion. ----
c
      MaSIN2= (Ma*DSIN(theta))**2
      Mb= DSQRT(((gamma+1.0)**2*Ma*Ma*MaSIN2 - 4.0*(Masin2-1.0)
     $ *(gamma*Masin2+1.0))/(2.0*gamma*Masin2-(gamma-1.0))/
     $ ((gamma-1.0)*Masin2+2.0))
      ptb= pb*(1.0+(gamma-1.0)/2.0*Mb*Mb)**(gamma/(gamma-1.0))
      CALL EXPANS(Mb,ptb,delta, Md,pd, gamma)
c
c--- Solve the lower control volume for pe, Ue, and Te.---
c
      le= lc
      pe= pd
      Ue= (2.0*mdoti*(Cp*Ti + Ui*Ui/2.0))/
     $ (pb*lc - pe*le + mdoti*Ui*COS(deltai) + 2.0*pe*le*Cp/R)
      Te= (pe*Ue**3*le)/2.0/R/(mdoti*(Cp*Ti+Ui*Ui/2.0) - pe*Ue*le*Cp/R)
      Me= Ue/DSQRT(gamma*R*Te)
      mdote= pe/R/Te*Ue*le
      mddif= mdoti - mdote
      RETURN
      END
c
c*********************************************************************************
c
      SUBROUTINE EXPANS (M1,pt,d, M2,p2, gamma)
      Implicit Real*8 (a-h,m,l,o-z)
c
c   This subroutine calculates the Mach number and pressure after a
c   Prandtl-Meyer expansion of angle 'd'.  Function subroutines 'DIF'
c   and 'NU' are part of this subroutine.
c
      dM= 0.05
      M2= M1 +.2
c
   10 DIFNOM=DIF(gamma,M1,M2,d)
      IF(DABS(DIFNOM).LT.0.0017) GO TO 100
      M2= M2-(DIFNOM*2.0*dM)/(DIF(gamma,M1,M2+dM,d)-
     $ DIF(gamma,M1,M2-dM,d))
      GO TO 10
  100 p2= pt/(1.0 + (gamma-1.0)/2.0*M2**2)**(gamma/(gamma-1.0))
      RETURN
      END
c
      FUNCTION DIF(gamma,M1,M2,d)
      Implicit Real*8 (a-h,m,l,o-z)
      Real*8 NU
```

61

```fortran
        DIF=NU( gamma,M2 )-( d+NU( gamma,M1 ))
        RETURN
        END
C
        FUNCTION NU( gamma,M )
        Implicit Real*8 (a-h,m,l,o-z)
        Real*8 NU
        b=( gamma+1 )/( gamma-1 )
        c=M**2-1.0
        NU=( DSQRT( b )*DATAN( DSQRT( c/b ))-DATAN( DSQRT( C )))
        RETURN
        END
C
C***************************************************************************
C
        SUBROUTINE MDEDFF( mdedif,uup,fup,ud,Td,c,le,hti,mdoti,Cp,R,pe,
      $ au,bu,cu,du, aT,bT,cT,dT, Vw)
        Implicit Real*8 (a-h,m,l,o-z)
C
C    This subroutine numerically integrates the mass flow in the 'f' profile
C        and slipline profile region.
C
        yup=le*( 1.0-fup )
        yd= le*( 1.0+fup )
        Vw= DSQRT( uup**2/( 1.0-fup**2-2.0*c*DLOG( fup )))
        Teup= ( hti-uup**2/2.0 )/Cp
        zT= -Vw**2/Cp/le*( fup+c/fup )
        CALL COEF( yd,yup,zT,Td,Teup, aT,bT,cT,dT )
        zu= Vw*( fup+c/fup )/le/DSQRT( 1.0-fup**2-2.0*c*DLOG( fup ))
        CALL COEF( yd,yup,zu,ud,uup, au,bu,cu,du )
C
C--- integrate the mass flow profile in region e -----------
C
C--- integrate the region below the slipline ----
C
        df= ( 1.0-fup )/200.0
        sum1= 0.0
        Do 101 k=1,200
        ak= k
        f= ( ak-0.5 )*df + fup
        sub= 1.0 - f**2 -2.0*c*DLOG( f )
  101 sum1= sum1 + Vw*DSQRT( sub )/( hti-Vw**2/2.0*sub )*df
        mdotl= pe*le*Cp/R*sum1
C
C--- integrate the massflow in the slipline ----
C
        dy= ( le-yup )/100.0
        sum2= 0.0
        Do 102 k=1,100
        ak= k
        y= ( ak-0.5 )*dy + yup
        us=  au*y**3 + bu*y**2 + cu*y + du
        Tes= aT*y**3 + bT*y**2 + cT*y + dT
```

```fortran
  102 sum2= sum2 + us/Tes*dy
      mdots= pe/R*sum2
      mdote= mdotl + mdots
      mdedif= mdoti-mdote
      RETURN
      END
c
c*********************************************************************************
c
      SUBROUTINE COEF(yd,yu,b2,b3,b4, aa,bb,cc,dd)
      Implicit Real*8 (a-h,m,l,o-z)
      Real*8 A(4,4),b(4)
c
c     This subroutine inverts a four by four matrix in order to solve for
c         the coeficients of the third order polynomial used to model the
c         velocity and temperature profile through the slipline.
c
      A(1,1)= 3.*yd**2
      A(1,2)= 2.*yd
      A(1,3)= 1.0
      A(1,4)= 0.0
      A(2,1)= 3.*yu**2
      A(2,2)= 2.*yu
      A(2,3)= 1.0
      A(2,4)= 0.0
      A(3,1)= yd**3
      A(3,2)= yd**2
      A(3,3)= yd
      A(3,4)= 1.0
      A(4,1)= yu**3
      A(4,2)= yu**2
      A(4,3)= yu
      A(4,4)= 1.0
      b(1)= 0.0
      b(2)= b2
      b(3)= b3
      b(4)= b4

      Do 122 k=1,3
      Do 122 i=k+1,4
      amult= A(i,k)/A(k,k)
      Do 123 j=k+1,4
  123 A(i,j)= A(i,j)-A(k,j)*amult
      A(i,k)=0.0
  122 b(i)= b(i)-b(k)*amult
c
c---- back solve -----
c
      b(4)=b(4)/A(4,4)
      Do 124 k=3,1,-1
      sum=0.0d0
      Do 125 j=k+1,4
  125 sum= A(k,j)*b(j)+sum
```

```
  124 b(k)= (b(k)-sum)/A(k,k)

      dd=b(4)
      cc=b(3)
      bb=b(2)
      aa=b(1)
      RETURN
      END
c
c**********************************************************************
c
      FUNCTION YLAWDF(y,Vw,le,c,visc)
      Implicit Real*8 (a-h,m,l,o-z)
c
c     This subroutine returns the difference between the RHS and LHS of
c        the law-of-the-wall equation  u+*y+ = U*y/nu  to the portion of
c        the main program seeking to find the value of y which makes this
c        difference zero.
c
      yplus= 10.
      uplus= 10.
      IF((y .LT. 0.0d0) .OR. (y .GT. le))GO TO 83
      f= 1.0-y/le
      u= Vw*DSQRT(1.0-f**2-2.0*c*DLOG(f))
      ylawdf= u*y/visc - uplus*yplus
      Return
   83 Write(*,409)y,le
  409 Format(' y is out of bounds in Subroutine YLAWDF. y must be  0.0 <
     $ y < le .',/,' y= ',d12.5,'    le= ',d12.5)
      STOP
      End
c
c**********************************************************************
c
      SUBROUTINE INPUTD(title,xu,xl,pd,ud,hw,hd,n)
      Implicit Real*8(a-h,o-z)
      INTEGER GEOM,FLUID,SPACE,OUTPUT,MODE
      Character*72 title
c
c    This subroutine sets up the TEXSTAN input file 'DATA' which governs
c       geometry, boundary conditions, flow conditions, turbulence models,
c       and input/output instructions.  See TEXSTAN manual for details.
c
      OPEN(7,file='DATA',status='unknown')
      WRITE (7,100) title
  100 Format(' ',A72,'    ')

      geom=1
      mode=2
      fluid=2
      neq=2
      kex=2
      kin=2
```

```
kin=1
kent=1
kstart=0
kkd=10
WRITE (7,110) GEOM,MODE,FLUID,NEQ,N,KEX,KIN,KENT,KSTART,KKD

deltax=0.4
retran=200.0
fra=0.05
enfra=0.005
gv=0.0d0
WRITE (7,120) XU,XL,DELTAX,RETRAN,FRA,ENFRA,GV

i1=1
Write(7,110)i1,i1

rhoc=1.0
viscoc=.10d-04
prc=0.7
WRITE (7,120) Pd,RHOC,VISCOC,PRC

i2=2
Write(7,110)i2,i1
Write(7,110)i2,i1

a1=1.0d0
a0=0.0d0
Write(7,120)xu,a1,a0,a0,a0
Write(7,120)xl,a1,a0,a0,a0
Write(7,120)a0,a0,hw
Write(7,120)ud,a0,hd
Write(7,120)a0,a0,hw
Write(7,120)ud,a0,hd

ak= 0.41
almgg=0.085
fr=0.01
aq=0.0d0
bq=0.0d0
ypmax=50.0
ypmin=20.0
WRITE (7,120) AK,ALMGG,FR,AQ,BQ,YPMAX,YPMIN

apll=25.0
bpll=0.0
signal=1.0
WRITE (7,120) APLL,BPLL,SIGNAL

pplag=4000.0
prt=0.90
Write(7,120)pplag,prt

cg=32.2
```

```fortran
      cj=779.0
      Write(7,120)cg,cj,a0,a0,a0,a0,a0
      numrun=1
      space=10000
      output=2
      k1=0
      k2=3
      k3=0
      k4=0
      k5=0
      k6=0
      k7=0
      k8=0
      k9=99
      k10=0
      k11=0
      k12=0
      k13=0
      WRITE(7,110)NUMRUN,SPACE,OUTPUT,K1,K2,K3,K4,K5,K6,K7,K8,K9,K10,
     $      K11,K12,K13
  110 Format(16(I5))
  120 Format(8(G10.4))
      Rewind 7
      Close (7)
      Return
      End
c
c***********************************************************************
c
      FUNCTION VISC(TR,p)
      Implicit Real*8 (a-h,l,m,o-z)

c   Calculation of kinematic viscosity.  Dynamic viscosity (mu) is determined
c        as a function of temperature below 3000 K from the relation in
c        Bertin and Smith.  Mu is not dependent on pressure in this range.
c
      R= 1717.93
      TK= TR/1.8
      mu= 1.458d-06 / 47.88026 * tk**1.5/(tk+110.4)
      visc= mu/p*R*TR
      Return
      End
```

66

Appendix C

Sample Input

Input data for "inj.for"

```
output file= Rozycki.out
1.     gamma= 1.4
2.        Cp= 6008.61    ft*lbf/slug/R
3.         R= 1717.9344 ft*lbf/slug/R
4.        Ma= 4.38
5.       pta= 29088.     psf
6.       Tta= 560.0      R
7.        Ti= 560.0      R
8.        li= 0.25       ft
9.    deltid= 90.0       deg
10.   lambda= 0.0153
11.       xl= 0.9405     ft
12.   slipfr= 0.03
13.   TEXSTAN output file title (72 char)=
 Rozycki:Academy Test
```

Appendix D

Sample Output

Rozycki:Academy Test

Ma= 4.38 Ua(ft/s)=2311.3 pa(psf)= 116.9 pta(psf)=   29088.0
Ta(R)= 115.8 Tta(R)= 560.0

Contact surface ('wedge') angle delta(deg)= 8.1

mdoti(slug/s)=0.00520 lambda=0.0153 pi(psf)= 265.6 Ui(ft/s)= 75.3
Ti(R)= 560.0 deltai(deg)= 90.0 li(ft)=0.2500

Md= 4.34 Ud(ft/s)=2306.4 pd(psf)= 117.0 ptd(psf)= 27516.1
Td(R)= 117.7 Ttd(R)= 560.0

Me= 0.95 Ue(ft/s)=1017.5 pe(psf)= 117.0 Te(R)= 474.3
le(ft)=0.0356

Reynolds Nu. at Station E =0.4163E+07

Boundary layer thicknesses at xl(ft)= 0.94 without   injection
delta99(in)= 0.1550   displacement delta1(in)= 0.0194   momentum delta2(in)= 0.0151

Momentum at Station 'e'
1-D (lbf)=   9.45   'f' Profile (lbf)=   10.52
percent difference =   11.4

Energy at Station 'e'
1-D (Btu/s)=   22.49   'f' Profile (Btu/s)=   22.44
percent difference=   0.2

1   Rozycki:Academy Test

GEOMETRY MODE FLUID NEQ N   KEX KIN KENT KSTART KKD
    1   2   6   2 70   2   1   1   0   10

ENTRAINMENT BASED ON BEHAVIOR OF ALL EQUATIONS.

     XU   XL   DELTAX   TRAN. RE NO.   FRA   ENFRA   GRAVITY CONST.
  0.2856E+00 0.9405E+00 0.4000E+00 0.2000E+03 0.5000E-01 0.5000E-02   0.0000E+00

BODY-FORCE SOURCE(1) SOURCE(2) SOURCE(3) SOURCE(4) SOURCE(5)
    1   1   .

68

```
        PRESSURE      DENSITY     VISCOSITY      PRC(1)      PRC(2)      PRC(3)

   THE FLUID IS NITROGEN
    0.1170E+03   0.1000E+01   0.1000E-04   0.7000E+00


   BOUNDARY CONDITIONS ALONG I- AND E-SURFACES
   NXBC      TYPBC1     TYPBC2     TYPBC3     TYPBC4     TYPBC5
    2           1
    2           1


   M    X(M)      RW(M)     AUX1(M)    AUX2(M)    AUX3(M)     UG(M)     AM(K,J)   FJ(K,1,M) FJ(K,2,M) FJ(K,3,M)
   1 0.2856E+00 0.1000E+01 0.0000E+00 0.0000E+00 0.0000E+00 0.2306E+04 0.0000E+00 0.1343E+03
                                                                       0.0000E+00 0.2822E+02
   2 0.9405E+00 0.1000E+01 0.0000E+00 0.0000E+00 0.0000E+00 0.2306E+04 0.0000E+00 0.1343E+03
                                                                       0.0000E+00 0.2822E+02


INITIAL PROFILES

   I       Y(I)        U(I)       F(1,I)      F(2,I)      F(3,I)
   1 0.000000E+00 0.000000E+00 0.134300E+03
   3 0.228200E-02 0.262800E+03 0.133100E+03
   4 0.303900E-02 0.304900E+03 0.132600E+03
   5 0.379500E-02 0.342600E+03 0.132100E+03
   6 0.455100E-02 0.377400E+03 0.131600E+03
   7 0.530700E-02 0.410000E+03 0.131100E+03
   8 0.606300E-02 0.440800E+03 0.130500E+03
   9 0.681900E-02 0.470400E+03 0.130000E+03
  10 0.757500E-02 0.498900E+03 0.129500E+03
  11 0.833200E-02 0.526600E+03 0.128900E+03
  12 0.908800E-02 0.553600E+03 0.128300E+03
  13 0.984400E-02 0.580100E+03 0.127700E+03
  14 0.106000E-01 0.606200E+03 0.127100E+03
  15 0.113600E-01 0.631900E+03 0.126500E+03
  16 0.121100E-01 0.657300E+03 0.125800E+03
  17 0.128700E-01 0.682600E+03 0.125100E+03
  18 0.136200E-01 0.707800E+03 0.124400E+03
  19 0.143800E-01 0.733000E+03 0.123700E+03
  20 0.151400E-01 0.758200E+03 0.123000E+03
  21 0.158900E-01 0.783500E+03 0.122200E+03
  22 0.166500E-01 0.808900E+03 0.121400E+03
  23 0.174100E-01 0.834500E+03 0.120500E+03
  24 0.181600E-01 0.860400E+03 0.119700E+03
  25 0.189200E-01 0.886700E+03 0.118700E+03
  26 0.196700E-01 0.913300E+03 0.117800E+03
  27 0.204300E-01 0.940400E+03 0.116800E+03
  28 0.211900E-01 0.968100E+03 0.115700E+03
  29 0.219400E-01 0.996500E+03 0.114600E+03
  30 0.227000E-01 0.102600E+04 0.113400E+03
  31 0.234500E-01 0.105600E+04 0.112200E+03
  32 0.242100E-01 0.108700E+04 0.110900E+03
  33 0.249700E-01 0.111900E+04 0.109400E+03
  34 0.257200E-01 0.115200E+04 0.107900E+03
  35 0.264800E-01 0.118800E+04 0.106300E+03
```

```
36 0.272400E-01 0.122500E+04 0.104500E+03
37 0.279900E-01 0.126400E+04 0.102500E+03
38 0.287500E-01 0.130600E+04 0.100400E+03
39 0.295000E-01 0.135200E+04 0.979600E+02
40 0.302600E-01 0.140200E+04 0.952200E+02
41 0.310200E-01 0.145700E+04 0.920600E+02
42 0.317700E-01 0.152000E+04 0.883200E+02
43 0.320200E-01 0.154400E+04 0.868400E+02
44 0.322800E-01 0.156900E+04 0.851700E+02
45 0.325300E-01 0.159700E+04 0.833100E+02
46 0.327800E-01 0.162600E+04 0.812900E+02
47 0.330300E-01 0.165700E+04 0.791100E+02
48 0.332900E-01 0.168800E+04 0.768100E+02
49 0.335400E-01 0.172100E+04 0.744000E+02
50 0.337900E-01 0.175500E+04 0.718900E+02
51 0.340400E-01 0.178900E+04 0.693000E+02
52 0.343000E-01 0.182400E+04 0.666500E+02
53 0.345500E-01 0.185900E+04 0.639600E+02
54 0.348000E-01 0.189400E+04 0.612500E+02
55 0.350600E-01 0.192900E+04 0.585300E+02
56 0.353100E-01 0.196400E+04 0.558200E+02
57 0.355600E-01 0.199800E+04 0.531400E+02
58 0.358100E-01 0.203100E+04 0.505000E+02
59 0.360700E-01 0.206300E+04 0.479300E+02
60 0.363200E-01 0.209500E+04 0.454300E+02
61 0.365700E-01 0.212400E+04 0.430400E+02
62 0.368200E-01 0.215300E+04 0.407600E+02
63 0.370800E-01 0.217900E+04 0.386200E+02
64 0.373300E-01 0.220400E+04 0.366200E+02
65 0.375800E-01 0.222600E+04 0.348000E+02
66 0.378300E-01 0.224600E+04 0.331600E+02
67 0.380900E-01 0.226400E+04 0.317200E+02
68 0.383400E-01 0.227900E+04 0.305100E+02
69 0.385900E-01 0.229000E+04 0.295300E+02
70 0.388400E-01 0.229900E+04 0.288200E+02
71 0.391000E-01 0.230500E+04 0.283700E+02
73 0.393500E-01 0.230600E+04 0.282200E+02
```

TURBULENCE CONSTANTS

KAPPA	LAMBDA	FR	AQ	BQ	MAX YPL WF	MIN YPL WF
0.4100E+00	0.8500E-01	0.1000E-01	0.0000E+00	0.0000E+00	0.5000E+02	0.2000E+02

APL	XXX	SIGNAL	PPLAG	PRT(1)	PRT(2)	PRT(3)
0.2500E+02	0.0000E+00	0.1000E+01	0.4000E+04	0.9000E+00		

DIMENSIONING SYSTEM CONSTANTS			ARBITRARY CONSTANTS			
G-SUB-C	J-SUB-C	AXX	BXX	CXX	DXX	EXX
0.3220E+02	0.7780E+03	0.0000E+00	0.0000E+00	0.0000E+00	0.0000E+00	0.0000E+00

NO. OF RUNS OF DATA	PRINTOUT SPACING	OUTPUT OPTION	K1	K2	K3	K4	K5	K6	K7	K8	K9	K10	K11	K12	K13
1	****	2	0	3	0	0	0	0	0	0	99	0	0	0	0

IF REM IS LESS THAN ABOUT 6000, LAMBDA IS MODIFIED BY AN INTERNAL CORRELATION
PRT (FOR THE ENERGY EQ) NEAR A WALL IS BEING EVALUATED BY AN INTERNAL CORRELATION

ROUTINE LAMSUB HAS BEEN CALLED
N HAS SHIFTED TO 69 AT INTG =   0

ROUTINE LAMSUB HAS BEEN CALLED
N HAS SHIFTED TO 68 AT INTG =   0

ROUTINE LAMSUB HAS BEEN CALLED
N HAS SHIFTED TO 67 AT INTG =   0

  FLOW IS TURBULENT
  USING PRANDTL MIXING-LENGTH TURB. MODEL
  USING VAN-DRIEST EXPONENTIAL DAMPING FUNCTION IN THE INNER REGION
  MODIFYING LAMBDA AT LOW-RE

  INTG   XU   UGU   K   F   REM   CF2   H   REH   ST   F(1,WALL)   A
ME   EXX
=   0 0.2856E+00 0.2306E+04 -.367E-09 0.000E+00 0.5494E+04 0.7169E-04 0.3207E+01 0.6040E+05 0.1461E-02 0.1343E+03 0.00
0E+00 0.223E+03

I	Y(I)	U(I)	F(1,I)	F(2,I)	F(3,I)	YPLUS(I)	UPLUS(I)	HPLUS(I)
1	0.0000E+00	0.0000E+00	0.1343E+03	0.0000E+00	0.0000E+00	0.0000E+00	0.0000E+00	0.0000E+00
2	0.2000E-02	0.1111E+03	0.1344E+03	0.0000E+00	0.0000E+00	0.1272E+02	0.5690E+01	0.0000E+00
3	0.6174E-02	0.3774E+03	0.1344E+03	0.0000E+00	0.0000E+00	0.3925E+02	0.1933E+02	0.0000E+00
4	0.6930E-02	0.4100E+03	0.1345E+03	0.0000E+00	0.0000E+00	0.4406E+02	0.2100E+02	0.0000E+00
5	0.7686E-02	0.4408E+03	0.1344E+03	0.0000E+00	0.0000E+00	0.4886E+02	0.2258E+02	0.0000E+00
6	0.8442E-02	0.4704E+03	0.1344E+03	0.0000E+00	0.0000E+00	0.5367E+02	0.2410E+02	0.0000E+00
7	0.9198E-02	0.4989E+03	0.1345E+03	0.0000E+00	0.0000E+00	0.5848E+02	0.2556E+02	0.0000E+00
8	0.9955E-02	0.5266E+03	0.1344E+03	0.0000E+00	0.0000E+00	0.6329E+02	0.2698E+02	0.0000E+00
9	0.1071E-01	0.5536E+03	0.1344E+03	0.0000E+00	0.0000E+00	0.6809E+02	0.2836E+02	0.0000E+00
10	0.1147E-01	0.5801E+03	0.1344E+03	0.0000E+00	0.0000E+00	0.7290E+02	0.2972E+02	0.0000E+00
11	0.1222E-01	0.6062E+03	0.1344E+03	0.0000E+00	0.0000E+00	0.7771E+02	0.3105E+02	0.0000E+00
12	0.1298E-01	0.6319E+03	0.1345E+03	0.0000E+00	0.0000E+00	0.8254E+02	0.3237E+02	0.0000E+00
13	0.1373E-01	0.6573E+03	0.1344E+03	0.0000E+00	0.0000E+00	0.8731E+02	0.3367E+02	0.0000E+00
14	0.1449E-01	0.6826E+03	0.1344E+03	0.0000E+00	0.0000E+00	0.9214E+02	0.3497E+02	0.0000E+00
15	0.1524E-01	0.7078E+03	0.1344E+03	0.0000E+00	0.0000E+00	0.9691E+02	0.3626E+02	0.0000E+00
16	0.1600E-01	0.7330E+03	0.1344E+03	0.0000E+00	0.0000E+00	0.1017E+03	0.3755E+02	0.0000E+00
17	0.1676E-01	0.7582E+03	0.1345E+03	0.0000E+00	0.0000E+00	0.1066E+03	0.3884E+02	0.0000E+00
18	0.1751E-01	0.7835E+03	0.1345E+03	0.0000E+00	0.0000E+00	0.1113E+03	0.4014E+02	0.0000E+00
19	0.1827E-01	0.8089E+03	0.1345E+03	0.0000E+00	0.0000E+00	0.1162E+03	0.4144E+02	0.0000E+00
20	0.1903E-01	0.8345E+03	0.1344E+03	0.0000E+00	0.0000E+00	0.1210E+03	0.4275E+02	0.0000E+00
21	0.1978E-01	0.8604E+03	0.1345E+03	0.0000E+00	0.0000E+00	0.1258E+03	0.4408E+02	0.0000E+00
22	0.2054E-01	0.8867E+03	0.1344E+03	0.0000E+00	0.0000E+00	0.1306E+03	0.4542E+02	0.0000E+00
23	0.2129E-01	0.9133E+03	0.1344E+03	0.0000E+00	0.0000E+00	0.1354E+03	0.4679E+02	0.0000E+00
24	0.2205E-01	0.9404E+03	0.1345E+03	0.0000E+00	0.0000E+00	0.1402E+03	0.4818E+02	0.0000E+00
25	0.2281E-01	0.9681E+03	0.1344E+03	0.0000E+00	0.0000E+00	0.1450E+03	0.4959E+02	0.0000E+00
26	0.2356E-01	0.9965E+03	0.1344E+03	0.0000E+00	0.0000E+00	0.1498E+03	0.5105E+02	0.0000E+00
27	0.2432E-01	0.1026E+04	0.1344E+03	0.0000E+00	0.0000E+00	0.1546E+03	0.5256E+02	0.0000E+00
28	0.2507E-01	0.1056E+04	0.1345E+03	0.0000E+00	0.0000E+00	0.1594E+03	0.5410E+02	0.0000E+00

```
29  0.2583E-01  0.1087E+04  0.1345E+03  0.0000E+00  0.0000E+00  0.1642E+03  0.5569E+02  0.0000E+00
30  0.2659E-01  0.1119E+04  0.1344E+03  0.0000E+00  0.0000E+00  0.1691E+03  0.5732E+02  0.0000E+00
31  0.2734E-01  0.1152E+04  0.1344E+03  0.0000E+00  0.0000E+00  0.1738E+03  0.5902E+02  0.0000E+00
32  0.2810E-01  0.1188E+04  0.1345E+03  0.0000E+00  0.0000E+00  0.1787E+03  0.6086E+02  0.0000E+00
33  0.2886E-01  0.1225E+04  0.1345E+03  0.0000E+00  0.0000E+00  0.1835E+03  0.6275E+02  0.0000E+00
34  0.2961E-01  0.1264E+04  0.1344E+03  0.0000E+00  0.0000E+00  0.1883E+03  0.6475E+02  0.0000E+00
35  0.3037E-01  0.1306E+04  0.1344E+03  0.0000E+00  0.0000E+00  0.1931E+03  0.6690E+02  0.0000E+00
36  0.3112E-01  0.1352E+04  0.1344E+03  0.0000E+00  0.0000E+00  0.1979E+03  0.6926E+02  0.0000E+00
37  0.3188E-01  0.1402E+04  0.1345E+03  0.0000E+00  0.0000E+00  0.2027E+03  0.7182E+02  0.0000E+00
38  0.3264E-01  0.1457E+04  0.1344E+03  0.0000E+00  0.0000E+00  0.2075E+03  0.7464E+02  0.0000E+00
39  0.3339E-01  0.1520E+04  0.1344E+03  0.0000E+00  0.0000E+00  0.2123E+03  0.7787E+02  0.0000E+00
40  0.3364E-01  0.1544E+04  0.1344E+03  0.0000E+00  0.0000E+00  0.2139E+03  0.7910E+02  0.0000E+00
41  0.3390E-01  0.1569E+04  0.1343E+03  0.0000E+00  0.0000E+00  0.2155E+03  0.8038E+02  0.0000E+00
42  0.3415E-01  0.1597E+04  0.1342E+03  0.0000E+00  0.0000E+00  0.2171E+03  0.8181E+02  0.0000E+00
43  0.3440E-01  0.1626E+04  0.1341E+03  0.0000E+00  0.0000E+00  0.2187E+03  0.8330E+02  0.0000E+00
44  0.3465E-01  0.1657E+04  0.1339E+03  0.0000E+00  0.0000E+00  0.2203E+03  0.8489E+02  0.0000E+00
45  0.3491E-01  0.1688E+04  0.1337E+03  0.0000E+00  0.0000E+00  0.2220E+03  0.8647E+02  0.0000E+00
46  0.3516E-01  0.1721E+04  0.1335E+03  0.0000E+00  0.0000E+00  0.2235E+03  0.8816E+02  0.0000E+00
47  0.3541E-01  0.1755E+04  0.1334E+03  0.0000E+00  0.0000E+00  0.2251E+03  0.8991E+02  0.0000E+00
48  0.3566E-01  0.1789E+04  0.1332E+03  0.0000E+00  0.0000E+00  0.2267E+03  0.9165E+02  0.0000E+00
49  0.3592E-01  0.1824E+04  0.1331E+03  0.0000E+00  0.0000E+00  0.2284E+03  0.9344E+02  0.0000E+00
50  0.3617E-01  0.1859E+04  0.1329E+03  0.0000E+00  0.0000E+00  0.2300E+03  0.9523E+02  0.0000E+00
51  0.3642E-01  0.1894E+04  0.1328E+03  0.0000E+00  0.0000E+00  0.2316E+03  0.9703E+02  0.0000E+00
52  0.3668E-01  0.1929E+04  0.1328E+03  0.0000E+00  0.0000E+00  0.2332E+03  0.9882E+02  0.0000E+00
53  0.3693E-01  0.1964E+04  0.1328E+03  0.0000E+00  0.0000E+00  0.2348E+03  0.1006E+03  0.0000E+00
54  0.3718E-01  0.1998E+04  0.1328E+03  0.0000E+00  0.0000E+00  0.2364E+03  0.1024E+03  0.0000E+00
55  0.3743E-01  0.2031E+04  0.1328E+03  0.0000E+00  0.0000E+00  0.2380E+03  0.1040E+03  0.0000E+00
56  0.3769E-01  0.2063E+04  0.1329E+03  0.0000E+00  0.0000E+00  0.2396E+03  0.1057E+03  0.0000E+00
57  0.3794E-01  0.2095E+04  0.1330E+03  0.0000E+00  0.0000E+00  0.2412E+03  0.1073E+03  0.0000E+00
58  0.3819E-01  0.2124E+04  0.1331E+03  0.0000E+00  0.0000E+00  0.2428E+03  0.1088E+03  0.0000E+00
59  0.3844E-01  0.2153E+04  0.1333E+03  0.0000E+00  0.0000E+00  0.2444E+03  0.1103E+03  0.0000E+00
60  0.3870E-01  0.2179E+04  0.1334E+03  0.0000E+00  0.0000E+00  0.2460E+03  0.1116E+03  0.0000E+00
61  0.3895E-01  0.2204E+04  0.1336E+03  0.0000E+00  0.0000E+00  0.2476E+03  0.1129E+03  0.0000E+00
62  0.3920E-01  0.2226E+04  0.1337E+03  0.0000E+00  0.0000E+00  0.2492E+03  0.1140E+03  0.0000E+00
63  0.3945E-01  0.2246E+04  0.1338E+03  0.0000E+00  0.0000E+00  0.2508E+03  0.1151E+03  0.0000E+00
64  0.3971E-01  0.2264E+04  0.1340E+03  0.0000E+00  0.0000E+00  0.2525E+03  0.1160E+03  0.0000E+00
65  0.3996E-01  0.2279E+04  0.1342E+03  0.0000E+00  0.0000E+00  0.2541E+03  0.1167E+03  0.0000E+00
66  0.4021E-01  0.2290E+04  0.1342E+03  0.0000E+00  0.0000E+00  0.2556E+03  0.1173E+03  0.0000E+00
67  0.4046E-01  0.2299E+04  0.1343E+03  0.0000E+00  0.0000E+00  0.2572E+03  0.1178E+03  0.0000E+00
68  0.4072E-01  0.2305E+04  0.1344E+03  0.0000E+00  0.0000E+00  0.2589E+03  0.1181E+03  0.0000E+00
69  0.4097E-01  0.2307E+04  0.1343E+03  0.0000E+00  0.0000E+00  0.2605E+03  0.1182E+03  0.0000E+00
70  0.4097E-01  0.2306E+04  0.1344E+03  0.0000E+00  0.0000E+00  0.2605E+03  0.1181E+03  0.0000E+00
```

```
  INTG    XU      UGU      K      F      REH     CF2      H      REH     ST    F(1,WALL)   A
ME    EXX
```

THE TURBULENT COUETTE WALL FUNCTION IS BEING USED, AT   LEAST AT THIS INTEGRATION

ROUTINE LAMSUB HAS BEEN CALLED
N HAS SHIFTED TO 68 AT INTG = 71

 = 81 0.9405E+00 0.2306E+04 0.000E+00 0.000E+00 0.5915E+04 0.1018E-02 0.1511E+01 0.5474E+05 -.2737E-02 0.1343E+03 -.34
8E-01 -.138E+04

I	Y(I)	U(I)	F(1,I)	F(2,I)	F(3,I)	YPLUS(I)	UPLUS(I)	HPLUS(I)
1	0.0000E+00	0.0000E+00	0.1343E+03	0.0000E+00	0.0000E+00	0.0000E+00	0.0000E+00	0.0000E+00
2	0.4689E-03	0.3207E+03	0.1343E+03	0.0000E+00	0.0000E+00	0.1123E+02	0.1116E+02	0.9351E-01
3	0.2256E-02	0.1136E+04	0.1342E+03	0.0000E+00	0.0000E+00	0.5403E+02	0.1545E+02	0.1351E-02
4	0.3826E-02	0.1240E+04	0.1342E+03	0.0000E+00	0.0000E+00	0.9165E+02	0.1686E+02	0.1473E-02
5	0.4517E-02	0.1273E+04	0.1342E+03	0.0000E+00	0.0000E+00	0.1082E+03	0.1731E+02	0.1503E-02
6	0.5246E-02	0.1304E+04	0.1342E+03	0.0000E+00	0.0000E+00	0.1257E+03	0.1773E+02	0.1543E-02
7	0.6008E-02	0.1332E+04	0.1342E+03	0.0000E+00	0.0000E+00	0.1439E+03	0.1811E+02	0.1591E-02
8	0.6803E-02	0.1359E+04	0.1342E+03	0.0000E+00	0.0000E+00	0.1630E+03	0.1847E+02	0.1598E-02
9	0.7629E-02	0.1383E+04	0.1342E+03	0.0000E+00	0.0000E+00	0.1827E+03	0.1881E+02	0.1608E-02
10	0.8483E-02	0.1407E+04	0.1342E+03	0.0000E+00	0.0000E+00	0.2032E+03	0.1913E+02	0.1641E-02
11	0.9365E-02	0.1429E+04	0.1342E+03	0.0000E+00	0.0000E+00	0.2243E+03	0.1943E+02	0.1643E-02
12	0.1027E-01	0.1451E+04	0.1342E+03	0.0000E+00	0.0000E+00	0.2461E+03	0.1973E+02	0.1683E-02
13	0.1121E-01	0.1472E+04	0.1342E+03	0.0000E+00	0.0000E+00	0.2686E+03	0.2001E+02	0.1666E-02
14	0.1216E-01	0.1493E+04	0.1342E+03	0.0000E+00	0.0000E+00	0.2914E+03	0.2030E+02	0.1677E-02
15	0.1315E-01	0.1515E+04	0.1342E+03	0.0000E+00	0.0000E+00	0.3151E+03	0.2060E+02	0.1689E-02
16	0.1415E-01	0.1538E+04	0.1342E+03	0.0000E+00	0.0000E+00	0.3389E+03	0.2091E+02	0.1709E-02
17	0.1518E-01	0.1562E+04	0.1342E+03	0.0000E+00	0.0000E+00	0.3636E+03	0.2124E+02	0.1717E-02
18	0.1623E-01	0.1587E+04	0.1342E+03	0.0000E+00	0.0000E+00	0.3888E+03	0.2157E+02	0.1724E-02
19	0.1729E-01	0.1612E+04	0.1342E+03	0.0000E+00	0.0000E+00	0.4141E+03	0.2191E+02	0.1712E+02
20	0.1837E-01	0.1638E+04	0.1342E+03	0.0000E+00	0.0000E+00	0.4401E+03	0.2227E+02	0.1712E+02
21	0.1948E-01	0.1664E+04	0.1342E+03	0.0000E+00	0.0000E+00	0.4665E+03	0.2263E+02	0.1692E+02
22	0.2058E-01	0.1691E+04	0.1342E+03	0.0000E+00	0.0000E+00	0.4930E+03	0.2299E+02	0.1687E+02
23	0.2172E-01	0.1718E+04	0.1342E+03	0.0000E+00	0.0000E+00	0.5202E+03	0.2337E+02	0.1662E+02
24	0.2286E-01	0.1746E+04	0.1342E+03	0.0000E+00	0.0000E+00	0.5475E+03	0.2374E+02	0.1643E+02
25	0.2402E-01	0.1774E+04	0.1342E+03	0.0000E+00	0.0000E+00	0.5755E+03	0.2412E+02	0.1599E+02
26	0.2521E-01	0.1803E+04	0.1342E+03	0.0000E+00	0.0000E+00	0.6038E+03	0.2451E+02	0.1559E+02
27	0.2639E-01	0.1831E+04	0.1342E+03	0.0000E+00	0.0000E+00	0.6322E+03	0.2489E+02	0.1512E+02
28	0.2761E-01	0.1859E+04	0.1342E+03	0.0000E+00	0.0000E+00	0.6613E+03	0.2528E+02	0.1453E+02
29	0.2882E-01	0.1888E+04	0.1342E+03	0.0000E+00	0.0000E+00	0.6904E+03	0.2567E+02	0.1399E+02
30	0.3007E-01	0.1917E+04	0.1342E+03	0.0000E+00	0.0000E+00	0.7203E+03	0.2606E+02	0.1330E+02
31	0.3134E-01	0.1945E+04	0.1342E+03	0.0000E+00	0.0000E+00	0.7507E+03	0.2645E+02	0.1243E+02
32	0.3261E-01	0.1974E+04	0.1342E+03	0.0000E+00	0.0000E+00	0.7811E+03	0.2683E+02	0.1160E+02
33	0.3391E-01	0.2002E+04	0.1343E+03	0.0000E+00	0.0000E+00	0.8124E+03	0.2722E+02	0.1060E+02
34	0.3524E-01	0.2030E+04	0.1343E+03	0.0000E+00	0.0000E+00	0.8442E+03	0.2760E+02	0.9536E+01
35	0.3657E-01	0.2057E+04	0.1343E+03	0.0000E+00	0.0000E+00	0.8761E+03	0.2797E+02	0.8306E+01
36	0.3795E-01	0.2084E+04	0.1343E+03	0.0000E+00	0.0000E+00	0.9091E+03	0.2834E+02	0.7000E+01
37	0.3934E-01	0.2111E+04	0.1343E+03	0.0000E+00	0.0000E+00	0.9423E+03	0.2870E+02	0.5587E+01
38	0.4078E-01	0.2137E+04	0.1343E+03	0.0000E+00	0.0000E+00	0.9768E+03	0.2905E+02	0.4062E+01
39	0.4225E-01	0.2162E+04	0.1343E+03	0.0000E+00	0.0000E+00	0.1012E+04	0.2939E+02	0.2467E+01
40	0.4375E-01	0.2186E+04	0.1343E+03	0.0000E+00	0.0000E+00	0.1048E+04	0.2972E+02	0.8157E+00
41	0.4426E-01	0.2193E+04	0.1343E+03	0.0000E+00	0.0000E+00	0.1060E+04	0.2982E+02	0.1824E+00
42	0.4480E-01	0.2201E+04	0.1343E+03	0.0000E+00	0.0000E+00	0.1073E+04	0.2993E+02	-.3913E+00
43	0.4532E-01	0.2209E+04	0.1343E+03	0.0000E+00	0.0000E+00	0.1086E+04	0.3003E+02	-.9981E+00
44	0.4586E-01	0.2216E+04	0.1343E+03	0.0000E+00	0.0000E+00	0.1098E+04	0.3013E+02	-.1645E+01
45	0.4640E-01	0.2223E+04	0.1343E+03	0.0000E+00	0.0000E+00	0.1111E+04	0.3023E+02	-.2205E+01
46	0.4697E-01	0.2231E+04	0.1343E+03	0.0000E+00	0.0000E+00	0.1125E+04	0.3033E+02	-.2881E+01
47	0.4753E-01	0.2238E+04	0.1343E+03	0.0000E+00	0.0000E+00	0.1139E+04	0.3042E+02	-.3438E+01
48	0.4810E-01	0.2244E+04	0.1343E+03	0.0000E+00	0.0000E+00	0.1152E+04	0.3051E+02	-.4085E+01
49	0.4868E-01	0.2251E+04	0.1343E+03	0.0000E+00	0.0000E+00	0.1166E+04	0.3060E+02	-.4732E+01
50	0.4930E-01	0.2257E+04	0.1343E+03	0.0000E+00	0.0000E+00	0.1181E+04	0.3069E+02	-.5375E+01
51	0.4990E-01	0.2263E+04	0.1343E+03	0.0000E+00	0.0000E+00	0.1195E+04	0.3077E+02	-.6061E+01

```
52  0.5051E-01  0.2269E+04  0.1343E+03  0.0000E+00  0.0000E+00  0.1210E+04  0.3085E+02  -.5668E+01
53  0.5116E-01  0.2275E+04  0.1343E+03  0.0000E+00  0.0000E+00  0.1225E+04  0.3093E+02  -.7321E+01
54  0.5179E-01  0.2280E+04  0.1343E+03  0.0000E+00  0.0000E+00  0.1241E+04  0.3100E+02  -.7931E+01
55  0.5243E-01  0.2285E+04  0.1343E+03  0.0000E+00  0.0000E+00  0.1256E+04  0.3106E+02  -.8525E+01
56  0.5308E-01  0.2289E+04  0.1343E+03  0.0000E+00  0.0000E+00  0.1271E+04  0.3112E+02  -.9069E+01
57  0.5377E-01  0.2293E+04  0.1343E+03  0.0000E+00  0.0000E+00  0.1288E+04  0.3118E+02  -.9619E+01
58  0.5444E-01  0.2297E+04  0.1343E+03  0.0000E+00  0.0000E+00  0.1304E+04  0.3122E+02  -.1011E+02
59  0.5511E-01  0.2299E+04  0.1343E+03  0.0000E+00  0.0000E+00  0.1320E+04  0.3126E+02  -.1054E+02
60  0.5580E-01  0.2302E+04  0.1344E+03  0.0000E+00  0.0000E+00  0.1337E+04  0.3130E+02  -.1093E+02
61  0.5652E-01  0.2304E+04  0.1344E+03  0.0000E+00  0.0000E+00  0.1354E+04  0.3132E+02  -.1126E+02
62  0.5722E-01  0.2305E+04  0.1344E+03  0.0000E+00  0.0000E+00  0.1371E+04  0.3134E+02  -.1148E+02
63  0.5792E-01  0.2306E+04  0.1344E+03  0.0000E+00  0.0000E+00  0.1388E+04  0.3135E+02  -.1163E+02
64  0.5864E-01  0.2306E+04  0.1344E+03  0.0000E+00  0.0000E+00  0.1405E+04  0.3135E+02  -.1166E+02
65  0.5939E-01  0.2306E+04  0.1344E+03  0.0000E+00  0.0000E+00  0.1423E+04  0.3135E+02  -.1166E+02
66  0.6011E-01  0.2306E+04  0.1344E+03  0.0000E+00  0.0000E+00  0.1440E+04  0.3135E+02  -.1165E+02
67  0.6083E-01  0.2306E+04  0.1344E+03  0.0000E+00  0.0000E+00  0.1457E+04  0.3135E+02  -.1166E+02
68  0.6156E-01  0.2306E+04  0.1344E+03  0.   00E+00  0.0000E+00  0.1475E+04  0.3135E+02  -.1166E+02
69  0.6232E-01  0.2306E+04  0.1344E+03  0.0000E+00  0.0000E+00  0.1493E+04  0.3135E+02  -.1166E+02
70  0.6305E-01  0.2306E+04  0.1344E+03  0.0000E+00  0.0000E+00  0.1510E+04  0.3135E+02  -.1166E+02
71  0.6305E-01  0.2306E+04  0.1344E+03  0.0000E+00  0.0000E+00  0.1510E+04  0.3135E+02  -.1166E+02
```

The boundary layer thicknesses at xl(ft)= 0.9405
delta99(in)= 0.6264   displacement delta1(in)= 0.3781   momentum delta2(in)= 0.0360

SECURITY CLASSIFICATION OF THIS PAGE

REPORT DOCUMENTATION PAGE

1a. REPORT SECURITY CLASSIFICATION UNCLASSIFIED		1b. RESTRICTIVE MARKINGS		
2a. SECURITY CLASSIFICATION AUTHORITY		3. DISTRIBUTION/AVAILABILITY OF REPORT Approved for public release; distribution unlimited.		
2b. DECLASSIFICATION/DOWNGRADING SCHEDULE				
4. PERFORMING ORGANIZATION REPORT NUMBER(S) AFIT/GAE/ENY/89D-04		5. MONITORING ORGANIZATION REPORT NUMBER(S)		
6a. NAME OF PERFORMING ORGANIZATION School of Engineering	6b. OFFICE SYMBOL (If applicable) AFIT/ENY	7a. NAME OF MONITORING ORGANIZATION		
6c. ADDRESS (City, State, and ZIP Code) Air Force Institute of Technology Wright-Patterson AFB, Ohio 45433-6583		7b. ADDRESS (City, State, and ZIP Code)		
8a. NAME OF FUNDING/SPONSORING ORGANIZATION Wright Research Develop Ctr	8b. OFFICE SYMBOL (If applicable) FIMM	9. PROCUREMENT INSTRUMENT IDENTIFICATION NUMBER		

8c. ADDRESS (City, State, and ZIP Code) Wright-Patterson AFB, Ohio 45433	10. SOURCE OF FUNDING NUMBERS			
	PROGRAM ELEMENT NO.	PROJECT NO.	TASK NO.	WORK UNIT ACCESSION NO.

11. TITLE (Include Security Classification)

A Computational Model For Thickening Boundary Layers With Mass Addition For Hypersonic Engine Inlet Testing

12. PERSONAL AUTHOR(S)

Robert D. Clausen, Capt, USAF

13a. TYPE OF REPORT Thesis	13b. TIME COVERED FROM _____ TO _____	14. DATE OF REPORT (Year, Month, Day) 1989 December	15. PAGE COUNT 83

16. SUPPLEMENTARY NOTATION

17. COSATI CODES			18. SUBJECT TERMS (Continue on reverse if necessary and identify by block number)
FIELD	GROUP	SUB-GROUP	Boundary Layers, Inlets, Mass Addition, Injection, Blowing
20	04		

19. ABSTRACT (Continue on reverse if necessary and identify by block number)

Thesis Advisor: Lt. Col. Paul I. King, Ph.D.
Assistant Professor of Aerospace Engineering

20. DISTRIBUTION/AVAILABILITY OF ABSTRACT ☒ UNCLASSIFIED/UNLIMITED ☐ SAME AS RPT. ☐ DTIC USERS	21. ABSTRACT SECURITY CLASSIFICATION UNCLASSIFIED	
22a. NAME OF RESPONSIBLE INDIVIDUAL Lt Col King, Assistant Professor of Aero. Eng.	22b. TELEPHONE (Include Area Code) (513)-255-4476	22c. OFFICE SYMBOL AFIT/ENY

DD Form 1473, JUN 86 Previous editions are obsolete. SECURITY CLASSIFICATION OF THIS PAGE

A computational model for thickening boundary layers with mass addition is developed. The phenomena of uniform injection into a two-dimensional supersonic stream and subsequent boundary layer growth downstream is discussed. Analysis of the injection region provides the thickness of the boundary layer just aft of injection. An injection region velocity profile is then used to approximate the boundary layer profile just aft of injection and is input into a finite-difference boundary layer code. Downstream profiles and thicknesses are calculated and compared to experimental results.

The computational model developed here provides a tool for the design of a boundary layer generation system for hypersonic engine inlet testing. This mass addition system is needed to simulate the boundary layer developed on the forebody of hypersonic vehicles. An example is discussed which increases the natural boundary layer thickness 17 times.